Coexistence of Photosynthetic Marine Microorganisms, Viruses, and Grazers: Toward Integration in Ocean Ecosystem Models

Paul Frémont [1,*], Stephen J. Beckett [1,2,*], David Demory [3], Eric Carr [4], Christopher L. Follett [5], David Talmy [4], Stephanie Dutkiewicz [6,7], and Joshua S. Weitz [1,2,8,*]

[1]Department of Biology, University of Maryland, College Park, MD, USA
[2]University of Maryland Institute for Health Computing, North Bethesda, MD, USA
[3]Sorbonne Université, CNRS, USR 3579, Laboratoire de Biodiversité et Biotechnologies Microbiennes (LBBM), Observatoire Océanologique, Banyuls-sur-Mer, France
[4]Department of Microbiology, University of Tennessee, Knoxville, Tennessee, USA
[5]Department of Earth, Ocean and Ecological Sciences, University of Liverpool, Liverpool, UK
[6]Department of Earth, Atmospheric, and Planetary Sciences, Massachusetts Institute of Technology, Cambridge, MA, USA
[7]Center for Sustainability Science and Strategy, Massachusetts Institute of Technology, Cambridge, MA, USA
[8]Department of Physics, University of Maryland, College Park, MD, USA

[*]Corresponding authors: pfremont@umd.edu, beckett@umd.edu, jsweitz@umd.edu

Abstract

Photosynthetic microorganisms are responsible for primary production at the base of the marine food web that shapes ocean biogeochemistry and ecology. The growth of these microorganisms is balanced by mortality, including top-down losses by microbial grazing by heterotrophic nanoflagellates and zooplankton and infection and lysis by viruses. Notably, multiple types of grazers and viruses often coexist despite apparent competition for the same (or similar) microorganisms. Here, we develop a community model of photosynthetic microorganisms, grazers, and viruses that accounts for molar cell and virion quotas suitable for incorporation into ocean ecosystem models. Our aim is to investigate mechanisms that enable coexistence of a virus and a grazer with a single phytoplankton type. To do so, we evaluate the extent to which coexistence is facilitated by: (i) the inclusion of an infected class of the phytoplankton, potentially subject to intraguild predation, where grazers feed on virally infected microorganisms; (ii) heterogeneity in susceptibility to infection, where microorganisms vary in their resistance to the virus either intracellularly or extracellularly; and (iii) the inclusion of higher-order mortality terms for the predators. When adding an infected class, we find evidence for a trade-off between the virus latent period and virulence in facilitating a coexistence regime. The inclusion of an explicit latent period can generate oscillations of all populations that facilitate coexistence by reducing the fitness of the free virus, or lead to system collapse when oscillations become too large. Heterogeneity in phage susceptibility promotes coexistence through resource partitioning between the predators, while quadratic mortality terms widen the coexistence regime by stabilizing the system. We observe strong sensitivity of the models' outcomes to the viral life history traits, including shifts in infected cell percentages and the balance between virally and zooplankton-induced mortality. Finally, taking advantage of algebraic calculation of model equilibria, we identify life history trait parameter combinations that yield realistic ecological properties in simplified oligotrophic and mesotrophic epipelagic environments. Importantly, our ecological models suggest that ongoing efforts to embed virus dynamics in large-scale ocean ecosystem models should include phytoplankton types that are moderately to strongly resistant to viral infection and lysis.

Key words

Marine ecology, Virus, Phytoplankton, Zooplankton, Coexistence, Biogeochemistry

Introduction

Marine phytoplankton are a diverse group of photosynthetic microorganisms at the base of the ocean food web (Field et al. 1998) that play a crucial role in various global biogeochemical cycles (Eppley et al. 1979) and are key contributors to the biological carbon pump (Henson et al. 2012; Guidi et al. 2015; Frémont et al. 2022). Phytoplankton are subject to multiple mortality mechanisms, including predation. These microorganisms are consumed by zooplankton such as heterotrophic nanoflagelattes (Zwirglmaier et al. 2009), dinoflagellates (Sherr et al. 1994), and copepods (Dussart 1965). Marine phytoplankton can also be infected by viruses, leading to the release of their cellular contents into the environment through cell lysis (Fuhrman et al. 1995; Wilhelm et al. 1999; Weitz 2015). Viruses are present at high densities, typically exceeding $10^{10}/L$ in marine surface waters (Wigington et al. 2016) and can be major drivers of phytoplankton mortality (Bergh et al. 1989; Proctor et al.

1990; Fuhrman et al. 1995; Suttle 2007; Mojica et al. 2016; Talmy et al. 2019b; Biggs et al. 2021; Carlson et al. 2022; Beckett et al. 2024) which, in turn, can lead to significant impacts on the flow of matter and nutrients (Wilhelm et al. 1999; Jover et al. 2014; Weitz et al. 2015; Guidi et al. 2015; Talmy et al. 2019a).

Current large-scale ocean biogeochemistry models include various forms of biological complexity in their representation of biological and inorganic components (Ilyina et al. 2013; Aumont et al. 2015; Séférian et al. 2020; Stock et al. 2020; Negrete-García et al. 2022). Some models incorporate comprehensive size-structured food webs, featuring numerous classes of phytoplankton, diazotrophs, mixotrophs, and several types of grazers (Dutkiewicz et al. 2020; Stock et al. 2020). The increasing complexity of these models has allowed the theoretical exploration of numerous processes on a large scale, such as the emergence of global patterns of phytoplankton diversity (Dutkiewicz et al. 2020), the impact of ocean acidification (Dutkiewicz et al. 2015a), or the importance of iron in the limitation of phytoplankton growth (Tagliabue et al. 2016). However, these large-scale models generally lack an explicit representation of the processes linked to phytoplankton infection by viruses, which has been recognized as an important future challenge (Mateus 2017). The parameterization and implementation of such models remain challenging due to the complexity of virus-host and virus-environment interactions. Critically, this challenge requires both experiments characterizing viral life history traits as well as *in situ* measurements of viral and phytoplankton concentrations to inform the models.

Datasets of experimental measurements of life history traits of phytoplankton viruses are available (Edwards et al. 2018; Edwards et al. 2021). They include burst size (the number of virions produced in a single viral infection), latent period (the time between infection and viral lysis), and adsorption rate (the rate of encounter at which an infection is produced). In particular, the adsorption rate of viruses can be highly variable and has been identified as crucial in the dynamics of viral infections (Talmy et al. 2019b). This parameter depends both on the size of the host and the virus in relation to the size dependence of Brownian motion (Berg et al. 1977). The swimming speed of preys also plays a key role (Murray et al. 1992; Talmy et al. 2019b; Edwards et al. 2021). For viruses, the adsorption rate can vary by several orders of magnitude and is typically less than (sometimes significantly less than) biophysical limits (Talmy et al. 2019b). Efforts are also underway to harmonize the inference of viral life history traits by combining *in vitro* experiments with dynamical models of viral infection (Hinson et al. 2023; Dominguez-Mirazo et al. 2024).

Likewise, *in situ* measurements of virus concentrations and infected cells (e.g., via the iPolony method (Mruwat et al. 2021; Carlson et al. 2022)) are increasingly common and can be used to compare viral-induced lysis to zooplankton grazing (Baudoux et al. 2007; Mojica et al. 2016; Carlson et al. 2022; Biggs et al. 2021; Beckett et al. 2024). For example, the observed infection percentage of *Prochlorococcus* cells is low in the North Pacific Subtropical gyre (NPSG), with cyanobacteria mortality dominated by zooplankton grazing (Mruwat et al. 2021; Beckett et al. 2024). However, other *in situ* studies have shown significant latitudinal variation in the relative contribution to mortality by viruses and grazers (Mojica et al. 2016; Carlson et al. 2022). In the North Pacific, a high percentage ($> 10\%$) of infected cyanobacteria has been consistently reported over multiple years in the transition zone between subtropical and subpolar gyres (Carlson et al. 2022). In the North Atlantic, virus-induced mortality of prokaryotes is an important factor at low and mid latitudes, while mortality associated with zooplankton dominated at higher latitudes ($> 56°$N) (Mojica et al. 2016). In eukaryotes, the grazing rates of *Phaeocystis* and picoeukaryotes have been shown to be dominated by viruses or zooplankton, but both rates were rarely found to be elevated simultaneously in the Southern Ocean (Biggs et al. 2021). These data suggest that in some cases viruses and zooplankton can tend to predominate over each other, where relative importance can vary depending on the eukaryotic phytoplankton group. For example, viral grazing has been found to be more important in cryptophytes, while zooplankton grazing was found to be more important in diatoms (Biggs et al. 2021). Finally, in the northeastern oligotrophic Atlantic, viral-induced mortality dominated in eukaryotes while zooplankton mortality dominated in prokaryotes (Baudoux et al. 2007).

Prior to incorporating viral lysis into large-scale biogeochemical models, it is crucial to first develop and understand these ecological models in simpler settings. Doing so allows for a clearer understanding of virus, grazer, and microbial dynamics. Multiple studies have begun to integrate viral lysis into biogeochemical models, exploring their behavior, and investigating various questions related to the ecology and biogeochemical roles of viral infections in the oceans (Fuhrman 1999; Weitz et al. 2015; Talmy et al. 2019b; Talmy et al. 2019a; Biswas et al. 2020; Demory et al. 2020; Demory et al. 2021; Beckett et al. 2024; Flynn et al. 2022). From a biogeochemical perspective, incorporating viral lysis into biogeochemical models is hypothesized to increase organic matter recycling through the viral "shunt", increase net primary production, and reduce energy transfer to higher trophic levels, such as zooplankton (Weitz et al. 2015). In a modeling study of the California Current Ecosystem (Talmy et al. 2019a), it was estimated that a significant portion of the carbon loss from grazing, including viral lysis, is redirected into nutrient recycling through viral lysates. However, this estimation comes with considerable uncertainty ($29 \pm 20\%$) (Talmy et al. 2019a). It also remains unclear to what extent viral lysis could enhance carbon export through the viral "shuttle" (Sullivan et al. 2017; Guidi et al. 2015; Zimmerman et al. 2020). Nevertheless, *in situ* observations suggest that this could be the case through the production of faster-sinking aggregates formed by lysis products (Yamada et al. 2018; Laber et al. 2018), and potentially through increased grazing on viral particles and infected cells (Zimmerman et al. 2020). Including viral lysis in large-scale biogeochemical models would enable exploration of the relative balance of virus versus grazer

impacts and "shunt" and "shuttle" mechanisms at planetary scales.

While a substantial body of literature explores the question of coexistence in ecological systems (Gause 1934; Hardin 1960; Armstrong et al. 1980; Chesson 1982; Polis et al. 1992; Holt et al. 1997; Huisman et al. 1999; Chesson 2000; Hin et al. 2011; Ellner et al. 2019; Yamamichi et al. 2022; Sieben et al. 2022; Orr et al. 2025), relatively few studies have examined how coexistence regimes emerge between viruses and zooplankton that both exploit phytoplankton as a resource (Levin et al. 1977; Weitz et al. 2015; Thingstad et al. 2019; Biswas et al. 2020; Flynn et al. 2022). In the case of the Lotka-Volterra model (Lotka 1920), the competitive exclusion principle applies to a system with two predators and one prey: one predator excludes the other (Armstrong et al. 1980). In resource competition models, increasing the complexity of the model by adding new resources can lead to chaotic behavior, where coexistence can emerge from such dynamics, as demonstrated in the case of the paradox of plankton (Huisman et al. 1999). Coexistence equilibria have also been investigated in host-virus systems with the inclusion of an infected class and explicit nutrients (Levin et al. 1977), as well as in multitrophic marine food webs, including zooplankton grazing (Weitz et al. 2015). Another theoretical study explored the role of selective grazing, where zooplankton avoid infected cells, in shaping the coexistence and dynamic behavior (chaotic or stable) of a model that includes a grazer, a free virus, and an infected class of phytoplankton (Biswas et al. 2020). An adaptive host fitness model that responds to high viral abundance by increasing viral resistance has also been proposed to facilitate the coexistence between viruses, grazers, and phytoplankton (Thingstad et al. 2019). Finally, the inclusion of parasites, such as viruses, is expected to increase the coexistence within plankton communities and, consequently, the diversity of marine food webs (Thingstad 2000; Dunne et al. 2013; Weitz et al. 2015; Flynn et al. 2022).

In this study, we first develop an elemental quota version of the **S**usceptible cell - **I**nfected cell - **V**irus (SIV) model (Levin et al. 1977; Weitz 2015) which is suitable for large-scale biogeochemical models accounting for cell and virion quotas. Including quotas provides a rationale for conversion between abundance (counts) and elemental concentration frameworks of viral ecology (Figure 1a). We develop extensions to this baseline model, including the addition of a grazing class, in order to explore how increasing ecological complexity (to include biologically relevant mechanisms) affects coexistence regimes for susceptible cells and their grazing and viral predators. We first explore the relevance of including an infected class (I) for the coexistence of the predators by comparing simplified models (SVZ and $SIVZ$, Figure 1c, d) across the virulence spectrum of the virus. Next, we incorporate mutations from the susceptible type (S) to an extracellular or intracellular resistant type in the $SVRZ$ and $SIVRZ$ models (Figure 1a, b), with varying resistance strengths, and examine the resulting coexistence regimes. Following this, we investigate the impact of including quadratic mortality terms, commonly used in biogeochemical models, for both viral and grazing predators. Finally, we define ecologically relevant concentrations and infection percentages, along with virus-induced mortality rates, that the system is expected to reach for simplified oligotrophic and mesotrophic epipelagic environments and for four types of phytoplankton (Figure 1b). We then compare these values to model output and life history trait models, and discuss the empirical and theoretical relevance of our results to improving understanding of the joint role of viral and grazing predation to ocean ecosystems.

Methods

From the SIV count model to the SIV elemental concentration model

We first convert the susceptible-infected-virus (SIV) count model (Levin et al. 1977; Weitz 2015), in units of individuals per volume, to an elemental concentration model, in units of nutrient molar concentrations (see Supplementary material for details of the calculation). In doing so, we write the viral "shunt" as a flux to the dissolved organic nitrogen (DON) pool and the viral "shuttle" as a flux to the particulate organic nitrogen (PON) pool but do not include the full microbial loop dynamics. The resulting SIV model for the virus-phytoplankton dynamics (and lysate fluxes to dissolved and particulate organic matter pools) can be written as follows:

$$\frac{dS}{dt} = \overbrace{\mu.S}^{\text{growth}} - \overbrace{d_S.S}^{\text{mortality}} - \overbrace{\frac{\epsilon_V.\phi_S}{Q_v}.S.V}^{\text{sucessful infection}} \tag{1a}$$

$$\frac{dI}{dt} = \overbrace{\frac{\epsilon_V.\phi_S}{Q_v}.S.V}^{\text{successful infection}} - \overbrace{d_S.I}^{\text{mortality}} - \overbrace{\frac{1}{\tau}.I}^{\text{lysis}} \tag{1b}$$

$$\frac{dV}{dt} = \overbrace{\frac{\beta}{\tau}.\frac{Q_v}{Q_p}I}^{\text{viral burst}} - \overbrace{d_V.V}^{\text{viral decay}} - \overbrace{\frac{\phi_S}{Q_p}.S.V}^{\text{adsorption}} \tag{1c}$$

$$J_{DON} = \overbrace{\gamma.\left(\frac{1}{\tau} - \frac{\beta}{\tau}.\frac{Q_v}{Q_p}\right).I}^{\text{shunt}} \tag{1d}$$

$$J_{PON} = \overbrace{(1-\gamma).\left(\frac{1}{\tau} - \frac{\beta}{\tau}.\frac{Q_v}{Q_p}\right).I}^{\text{shuttle}} \tag{1e}$$

In the above, μ is the division rate of susceptible cells (S), d_S is the cell mortality rate (natural cell death), ϕ_S is the adsorption rate of viruses to susceptible cells, ϵ_V represents an intracellular resistance to the virus - that is the fraction of adsorption events that lead to a successful infection - and d_V represents the decay rate of infectious virions. Infections have an average duration of τ, denoting the latent period, after which a burst size, β, of new virions are released into the environment. Q_p and Q_v are the respective nitrogen quota of the phytoplankton and the virus. The fluxes to the dissolved and particulate pools, J_{DON} and J_{PON} respectively, are included here for completeness though the microbial loop is not modeled explicitly but could be embedded as part of global ecosystem models (see Discussion for further details). Assuming a fixed stoichiometry, equation 1 also apply to other elements (*e.g.*, C or P) by substituting the nitrogen quota with the corresponding carbon or phosphorus quota, reflecting the different stoichiometry of viruses (Jover et al. 2014) and phytoplankton (Redfield 1934). We summarize the default set of parameters associated with all models in Table S1-3.

Elemental concentration models' equations: SVZ, $SIVZ$, $SVRZ$, $SIVRZ$

In this manuscript we explore four elemental concentration models based on the above framework: the SVZ, $SIVZ$, $SVRZ$ and $SIVRZ$ models. These extensions also include a zooplankton, Z, class; and the $SVRZ$ and $SIVRZ$ models include a resistant, R, subpopulation of cells with (partial or full) resistance to infection. The equations of the models are the following (for each model, we emphasize the added terms):

- SVZ

$$\frac{dS}{dt} = \overbrace{\mu.S}^{\text{growth}} - \overbrace{d_S.S}^{\text{mortality}} - \overbrace{\frac{\epsilon_V.\phi_S}{Q_v}.S.V}^{\text{infection}} - \overbrace{g_Z.Z.S}^{grazing} - \overbrace{\frac{S^2}{\tau_K.K}}^{\text{bottom-up control}} \tag{2a}$$

$$\frac{dV}{dt} = \overbrace{\frac{\beta.\epsilon_V.\phi_S}{Q_p}.S.V}^{\text{viral burst}} - \overbrace{d_V.V}^{\text{viral decay}} - \overbrace{\frac{\phi_S}{Q_p}.S.V}^{\text{viral adsorption}} - \overbrace{d_{V2}.V^2}^{higher-order\ losses} \tag{2b}$$

$$\frac{dZ}{dt} = \overbrace{\epsilon_Z.g_Z.S.Z}^{grazing} - \overbrace{d_Z.Z}^{mortality} - \overbrace{d_{Z2}.Z^2}^{higher-order\ losses}. \tag{2c}$$

- $SIVZ$

$$\frac{dS}{dt} = \mu.S - d_S.S - \frac{\epsilon_V.\phi_S}{Q_v}.S.V - g_Z.Z.S - \frac{S^2}{\tau_K.K} \tag{3a}$$

$$\frac{dI}{dt} = \overbrace{\frac{\epsilon_V.\phi_S}{Q_v}.S.V}^{\text{infection}} - \overbrace{d_S.I}^{\text{mortality}} - \overbrace{\frac{1}{\tau}.I}^{\text{lysis}} - \overbrace{g_Z.Z.I}^{\text{grazing}} \tag{3b}$$

$$\frac{dV}{dt} = \overbrace{\frac{\beta}{\tau}.\frac{Q_v}{Q_p}.I}^{\text{viral burst}} - d_V.V - \frac{\phi_S}{Q_p}.S.V - d_{V2}.V^2 \tag{3c}$$

$$\frac{dZ}{dt} = \epsilon_Z.g_Z.(S+I).Z - d_Z.Z - d_{Z2}.Z^2. \tag{3d}$$

- $SVRZ$

$$\frac{dS}{dt} = \mu.S - d_S.S - \frac{\epsilon_V.\phi_S}{Q_v}.S.V - g_Z.Z.S - \frac{S+R}{\tau_K.K}.S + \overbrace{\mu.r.(\zeta.R - S)}^{\text{mutation}} \tag{4a}$$

$$\frac{dR}{dt} = \overbrace{\mu.\zeta.R}^{\text{penalized growth}} - d_S.R - \frac{S+R}{\tau_K.K}.R - \overbrace{\frac{\epsilon_{VR}.\phi_R}{Q_v}.R.V}^{\text{reduced infection}} - g_Z.Z.R + \overbrace{\mu.r.(S - \zeta.R)}^{\text{mutation}} \tag{4b}$$

$$\frac{dV}{dt} = \frac{\beta.\epsilon_V.\phi_S}{Q_p}.S.V + \frac{\beta.\epsilon_{VR}.\phi_R}{Q_p}.R.V - d_V.V - \frac{\phi_S}{Q_p}.S.V - \frac{\phi_R}{Q_p}.S.V - d_{V2}.V^2 \tag{4c}$$

$$\frac{dZ}{dt} = \epsilon_Z.g_Z.(S+R).Z - d_Z.Z - d_{Z2}.Z^2. \tag{4d}$$

- $SIVRZ$

$$\frac{dS}{dt} = \mu.S - d_S.S - \frac{S+R}{\tau_K.K}.S - \frac{\epsilon_V.\phi_S}{Q_v}.S.V - g_Z.Z.S + \mu.r.(\zeta.R - S) \tag{5a}$$

$$\frac{dR}{dt} = \mu.\zeta.R - d_S.R - \frac{S+R}{\tau_K.K}.R - \frac{\epsilon_{VR}.\phi_R}{Q_v}.R.V - g_Z.Z.R + \mu.r.(S - \zeta.R) \tag{5b}$$

$$\frac{dI}{dt} = \frac{\epsilon_V.\phi_S}{Q_v}.S.V + \frac{\epsilon_{VR}.\phi_R}{Q_v}.R.V - d_S.I - \frac{1}{\tau}.I - g_Z.Z.I \tag{5c}$$

$$\frac{dV}{dt} = \frac{\beta}{\tau}.\frac{Q_v}{Q_p}.I - d_V.V - \frac{\phi_S}{Q_p}.S.V - \frac{\phi_R}{Q_p}.R.V - d_{V2}.V^2 \tag{5d}$$

$$\frac{dZ}{dt} = \epsilon_Z.g_Z.(S+I+R).Z - d_Z.Z - d_{Z2}.Z^2. \tag{5e}$$

The SVZ model, used as a baseline model, corresponds to the simplest predator-prey model, which represents viral infection and lysis as a simple predator (Lotka 1920). In all models, we include the following:

- A carrying capacity term, K for the phytoplankton, to approximate bottom-up control by nutrients which has relaxation time τ_K (see later section for an approximation with the resource-consumer model).
- Zooplankton grazing with a clearance rate g_Z, gross growth efficiency ϵ_Z, and a linear per capita mortality rate of d_Z.
- The potential for inclusion of quadratic mortality terms for the virus (d_{V2}) and the zooplankton (d_{Z2}) (see later sections for rationale).

Each model includes or does not include the I class ($SIVZ$ and $SIVRZ$ model) and/or a resistant type to the virus (R class, $SVRZ$ and $SIVRZ$ models). Models that include the I class introduce an additional parameter τ, the latent period of the virus, and a grazing term of the infected class by the zooplankton. The latter term also introduces intraguild predation of the virus (Holt et al. 1997). Models that include the R class introduce a mutation term, r, between the S and R class, extracellular resistance to the virus (through ϕ_R) and intracellular resistance to the virus for the R type (through ϵ_{VR}). Extracellular resistance is modeled as a reduction in the adsorption rate while intracellular resistance is modeled as a decrease in the probability of infection. Note that the grazing terms of the zooplankton could be written as follows:

$\frac{dS}{dt} = -\frac{\phi_Z}{Q_Z}.S.V$; $\frac{dI}{dt} = -\frac{\phi_Z}{Q_Z}.I.V$ and $\frac{dZ}{dt} = \frac{\epsilon_Z.\phi_Z}{Q_p}.(S+I).Z$
Which gives: $g_Z = \frac{\phi_Z}{Q_Z}$ and $\epsilon_Z = \epsilon_Z^{'}.\frac{Q_Z}{Q_p}$.
We summarize the default set of parameters associated with all models in Table S1-3.

Theoretical equilibria, stability and alternate stable states

For the SVZ model and the $SIVZ$ model, five possible equilibria are possible:

- S^*, I^*, V^*, Z^*
- $S^*, 0, 0, Z^*$
- $S^*, I^*, V^*, 0$
- $S^*, 0, 0, 0$
- $0, 0, 0, 0$.

For the $SVRZ$ and $SIVRZ$ model, eleven possible equilibria are possible:

- S^*, I^*, V^*, R^*, Z^*
- $S^*, I^*, V^*, \delta_{R^*}, Z^*$
- $\delta_{S^*}, I^*, V^*, R^*, Z^*$
- $S^*, I^*, V^*, \delta_{R^*}, 0$
- $S^*, I^*, V^*, R^*, 0$
- $\delta_{S^*}, I^*, V^*, R^*, 0$
- $S^*, 0, 0, \delta_{R^*}, Z^*$
- $\delta_{S^*}, 0, 0, R^*, Z^*$
- $S^*, 0, 0, \delta_{R^*}, 0$
- $\delta_{S^*}, 0, 0, R^*, 0$
- $0, 0, 0, 0$

Where δ_{X^*} is a state in which the variable X is in very low abundance: either S or R can be in such a state due to the mutation from one to another, while the other is abundant. Note that the five states where R is either 0 or δ_{R^*} can be mapped to the states of the $SIVZ$ and SVZ models.
For the purpose of finding ecologically relevant equilibria, we derive the five possible equilibria of the $SIVZ$ model (equation 3) and eleven of the $SIVRZ$ model (equation 5) in two cases (Supplementary Material):

- $d_{V2} = 0$ and $d_{Z2} > 0$
- $d_{V2} > 0$ and $d_{Z2} > 0$

We present the equilibria of the models including the I class – the equilibria of the other models can be calculated analogously and are included in the full model simulations.

Size and elemental quotas

Virus

For each class of phytoplankton, the size of the virus is set as the average size of viruses from the given group from the dataset of Edwards et al. 2018 (Table S1). Empirical elemental quota relationships for viral capsids are set from Jover et al. 2014:

$$Q_{virus}(N) = \frac{10^6}{N_A} \cdot \left(16(r_v - 2.5)^3 + 36(7.5r_v^2 - 18.75r_v + 15.63)\right) \cdot MMN, \tag{6}$$

where r_v is the radius of the virion, N_A is the Avogadro number and MMN is the molar mass of nitrogen.

Phytoplankton

For eukaryotes, we obtain nitrogen cell quotas following Menden-Deuer et al. 2000 and the Redfield ratio (Redfield 1934):

- Diatoms:

$$log_{10}(Q_{diatom}(C)) = (-0.541 + 0.811.log_{10}(Vol)), \tag{7}$$

- Eukaryotic protists excluding diatoms:

$$log_{10}(Q_{phytoeukaryotes}(C)) = (-0.665 + 0.939.log_{10}(Vol)), \tag{8}$$

where Vol is the cell volume. We then convert to nitrogen units ($\mu molN.cell^{-1}$):

$$Q(N) = Q(C).10^{-6}.\frac{1}{MMC}.\frac{16}{106} \tag{9}$$

where $\frac{16}{106}$ is the Redfield ratio of nitrogen to carbon and MMC is the molar mass of carbon.
For cyanobacteria, *Synechococcus* and *Prochlorococcus*, we use the carbon density of *Synechococcus* from Verity et al. 1992:

$$Q_{cyanobacteria}(N) = d.Vol.10^{-9}.\frac{1}{MMC}.\frac{16}{106}, \tag{10}$$

where d is the mass density of *Synechococcus*: d=470 fgC.μm^{-3}. Although Verity et al. 1992 fitted a relationship between cell size and carbon density, we use this value for both *Synechococcus* and *Prochlorococcus* because it was the smallest organism for which the density was measured.

Zooplankton

We consider a zooplankton with a 2.5 μm radius for cyanobacteria and 5 μm for a picoeukaryote and a diatom. We follow Menden-Deuer et al. 2000 for the size-structured elemental concentrations:

$$log_{10}(Q_{grazer}(C)) = (-0.547 + 0.9.log_{10}(Vol)). \tag{11}$$

Life history traits models and parameterization

Viruses: burst size, latent period, quadratic mortality and encounter rate

- **Burst size and latent period**

We used data from Edwards et al. 2018 to calibrate models of burst size as a function of different host and virus traits. Burst size ($\log_{10}$) was found to be the most highly correlated with host volume ($\log_{10}$) and secondarily with the radius of the virus. In addition to these predictors, we add the virus type (ssDNA, dsDNA, ssRNA) and the host type (prokaryote, diatom and eukaryotes) as predictors. Pairs of host type-virus type represented less than 5 times are also removed from the dataset. For eukaryotes, we exclude classes of eukaryotes represented less than four times in the dataset (Pelagophyte, Chlorophyte, Raphidophyte and Cryptophyte), leaving three classes of non diatom eukaryotes: Prasinopyte, Haptophyte and Dinoflagellates. We used leave-one-out cross validation (typically used for small datasets) (Hastie et al. 2009) to assess the performance of 4 types of models: linear models, generalized additive models (GAM) (Wood 2004), random forest (RF) (Breiman et al. 2012) and single-layer neural networks (NN) (Venables et al. 2002). The cross validation is also used to optimize the hyperparameters of the three latter models: the number of splines for GAM; the number of neurons, learning rate and seed for NN; the number of trees and the number of variables to randomly sample as candidates at each split for RF. The NN model performed the best on average to minimize the root mean square error (RMSE) in leave-one-out cross validation (Figure S1-4). The seed of the NN model for the latent period is not optimized as we empirically find that it overfit the dataset. The optimized NN models are used to set burst sizes and latent period (except for the burst size of diatom viruses where we instead used the GAM model due to apparent overfitting of the NN model (Figure S1-2)). Performances and fitting of the models are summarized for burst size in Figure S1-2 and latent period in Figure S3-4.

- **Quadratic mortality**

For the higher-order quadratic mortality term of the virus, we use the value of Beckett et al. 2024, that fitted a quadratic mortality for *Prochlorococcus* viruses at station ALOHA (Table S2). The quadratic mortality term, $d_{V2}.V^2$, for the virus represents losses due to unspecific binding to other particles present in the ocean, including self collisions and adsorption to particulate organic matter (POM).

- **Encounter rate**

We use an encounter rate kernel that assumes that the swimming speed of the phytoplankton is considered to have a multiplicative effect on the diffusion kernel (Murray et al. 1992; Edwards et al. 2021):

$$\phi_{th} = \overbrace{4.\pi.r_{phyto}.D_{virus}}^{\text{virus diffusion}} \cdot \overbrace{\frac{1}{2}.(1 + (1 + 2.\frac{u_{phyto}.r_{phyto}}{D_{virus}})^{1/3})}^{\text{phytoplankton swimming}}, \tag{12}$$

where r_{phyto} is the radius the phytoplankton. u_{phyto} is the swimming speed of the phytoplankton (defined below). D_{virus} is the diffusivity constant of the virus (defined below), the one of the phytoplankton being negligible in comparison. The diffusivity kernel of the virus is defined as follows (Einstein 1905):

$$D_{virus} = \frac{k_B.T}{6.\pi.\eta.r_{virus}}, \tag{13}$$

where k_B is the Boltzman constant, T is the temperature in Kelvin, η is the viscosity of water (taken to be 1 $kg.L^{-1}$). For the phytoplankton speed we use the following empirical model (Kiørboe 2011; Talmy et al. 2019b) for cyanobacteria and eukaryotes:

$$log_{10}(u_{phyto}) = 0.4 + 0.8.log_{10}(2r_{phyto}), \tag{14}$$

where r_{phyto} is in cm and u_{phyto} in $cm.s^{-1}$ (then converted in $m.s^{-1}$).

Phytoplankton: maximum growth rate and half saturation constant

For the maximum growth rates, we follow the empirical allometric relationship with cell volume from Dutkiewicz et al. 2020:

$$\mu_{max} = a_t.Vol^b, \tag{15}$$

in which a_t depends on the phytoplankton type (diatoms: 3.9, small eukaryotes: 1.4, cyanobacteria (*Prochlorococcus* and *Synechococcus*): 0.8). b is equal to -0.08 for diatoms and picoeukaryotes and 0.08 for cyanobacteria. For each of the four types (diatom, picoeukaryote, *Prochlorococcus* and *Synechococcus*), we consider a small cell of each type (Table S1). Each of them is infected by a virus of the average size of viruses from Edwards et al. 2018 from the respective categories (Table S1). The volume of the phytoplankton and the radius of the virus also allows to set the burst size and latent period of each virus. For the nutrient dependency, N_c the half saturation constant for growth is set as followed:

$$N_c = \frac{K.\mu_{max}.Q_{min}}{U_{max}}, \tag{16}$$

where K is the cell nutrient uptake half saturation constant, Q_{min} is the cell minimum stoichiometric quota, U_{max} is the maximal cell nutrient uptake rate. For all three parameters, an empirical allometric relationship with the cell volume Vol is used (see details in Dutkiewicz et al. 2020; Zakem et al. 2018).

Zooplankton predation

We parameterize zooplankton predation following Dutkiewicz et al. 2020. We consider a single zooplankton grazer with a grazing rate of 9.8 $(\mu molN.L^{-1})^{-1}.d^{-1}$, quadratic mortality of 1.4 $(\mu molN.L^{-1})^{-1}.d^{-1}$ and linear mortality of 0.067 d^{-1} (Dutkiewicz et al. 2020; Dutkiewicz et al. 2015b). Gross growth efficiency is set to 0.3 (Straile 1997). The quadratic mortality term, $d_{Z2}.Z^2$, represents higher order predation of the zooplankton which is not explicitly represented.

Simplified epipelagic environments

With the aim to better parameterize viral lysis models for large-scale biogeochemical models, we construct idealized epipelagic environments that account for their carrying capacity, temperature and nutrient limitation of growth and mortality terms and biotic limitation of grazing.

Approximation of the resource-consumer model by the carrying capacity model

In biogeochemical models, limiting resources for phytoplankton growth, *i.e.* nitrate, are explicitly represented. To simplify our model, we use a carrying capacity term. To make an equivalence between the two types of model we set the carrying capacity as the equilibrium concentration of the consumer in the resource-consumer model with a constant nutrient concentration. The resource-consumer model can be written as follow:

$$\frac{dP}{dt} = \mu.\frac{N}{N+N_c}.P - d.P \tag{17}$$

$$\frac{dN}{dt} = -\mu.\frac{N}{N+N_c}.P + w.(N_{deep} - N) \tag{18}$$

where P is the phytoplankton concentration, N the nutrient concentration, N_c is the half saturation constant, w is the surface-deep mixing rate and N_{deep} is the deep nutrient concentration, following Weitz et al. 2015. Assuming a constant nutrient concentration, we have:

$$P^* = w.(N_{deep} - N).\frac{N+N_c}{\mu.N} \tag{19}$$

P^* is used as the carrying capacity K in the carrying capacity model (Table S3 for parameter values).

Growth limitations

We define two typical epipelagic open ocean environments: oligotrophic and mesotrophic. To represent them in our models, in addition to modifying the carrying capacity, we add constant growth limitations:

- A constant penalty on the growth rate of the phytoplankton to represent changes in nutrient affinity considering a constant nutrient concentration. It is represented with a Michaelis–Menten term:

$$\mu = \mu(N) = \mu.\frac{N}{N+N_c}, \tag{20}$$

  where N_c is the half saturation constant.

- A constant penalty/advantage on the growth rates and all mortality parameters through modulation by temperature following the Eppley curve, parameterized with values from Dutkiewicz et al. 2020:

$$\gamma_T = \tau_T.e^{-A_T.(\frac{1}{T}-\frac{1}{T_N})}, \tag{21}$$

  where T is the temperature in Kelvin, τ_T, A_T, T_N are parameters regulating the maximum value and the shape of the limitation curve.

- The grazing rate of the zooplankton following a Hill function, with paramerization according to values in Dutkiewicz et al. 2020. We consider the carrying capacity as a large limit of phytoplankton concentration setting a constant grazing inhibition:

$$g_Z = g_Z(K) = g_Z.\frac{K^2}{K^2+S_c^2}. \tag{22}$$

We summarize the values chosen to be representative of the oligotrophic and mesopelagic environments, as well as the effects of these terms in Table S3.

Coexistence analysis

Predator growth rates

To analyze the mechanisms facilitating coexistence in the $SIVZ$ model, it is necessary to define the growth rates of the predators (Chesson 1982; Chesson et al. 1989; Ellner et al. 2019). The growth rate of the virus is set as the largest real part of the eigenvalues of the Jacobian J of the infected cell and virus, IV subsystem, with:

$$J = \begin{pmatrix} -\frac{1}{\tau} - d_S - g_z.Z & \frac{\phi_S.S}{Q_v} \\ \frac{\beta}{\tau}.\frac{Q_v}{Q_p} & -\frac{\phi_S.S}{Q_p} - d_v \end{pmatrix} \tag{23}$$

We can calculate the eigenvalues:

$$det(J - \lambda.I) = \lambda^2 - \lambda.(a+d) + a.d - b.c \tag{24}$$

with: $a = -\frac{1}{\tau} - d_S - g_z.Z$; $b = \frac{\phi_S.S}{Q_v}$; $c = \frac{\beta}{\tau}.\frac{Q_v}{Q_p}$ and $d = -\frac{\phi_S.S}{Q_p} - d_v$

The eigenvalues of J are a solution to the former quadratic equation. The largest eigenvalue is positive if $a.d - b.c < 0$ which is the condition for the virus growth rate to be positive.
The growth rate of the free virus is:

$$\mu_V = \frac{1}{V}.\frac{dV}{dt} = \frac{\beta}{\tau}.\frac{Q_v}{Q_p}.\frac{I}{V} - d_V - \frac{\phi_S}{Q_p}.S - d_{V2}.V \tag{25}$$

The growth rate of the zooplankton is:

$$\mu_Z = \epsilon_Z.g_Z.(S + I) - d_Z. \tag{26}$$

Modern coexistence theory

To assess the mechanisms of coexistence of the $SIVZ$ model (without quadratic mortality terms of the predators), we perform an invasion analysis following Ellner et al. 2019. Briefly, Modern Coexistence Theory (Ellner et al. 2019) shows that nonlinear responses to fluctuations in resources -either environmental or endogenous- can facilitate coexistence when species differ in how they respond to those fluctuations. Therefore, we calculate the differences in growth rates between the invader species and the resident species in the case of both invasion (virus invading and zooplankton invading), and for the different cases of constant/varying/covarying resources (I class and S class) (equation 12 from Ellner et al. 2019):

$$\Delta_j^X = \epsilon_{j\backslash j}^X - \epsilon_{k\backslash j}^X \tag{27}$$

where $\epsilon_{k\backslash j}^X$ denotes a term (see Ellner et al. 2019 for the complete definition based on the predators' growth rates) computed for species k when species j is the invader. X corresponds to the different cases of constant/varying/covarying resources:

- $X = 0$: both resources are constant (average over a periodic cycle from the simulation with species j as the invader);
- $X = S$: constant S;
- $X = I$: constant I;
- $X = (S\#I)$: independent variation of I and S;
- $X = (SI)$: covariance component.

For instance, the term Δ_Z^S is the *relative nonlinearity* in S for the zooplankton, *relative* in the sense that it reflects the difference in how the zooplankton (Z) and the virus (V) respond to fluctuations in the prey S. The average invasion growth rate of species j is the sum of all components:

$$\bar{r}_j = \sum_X \Delta_j^X. \tag{28}$$

Coexistence is possible in the case of mutual invasibility *i.e.* if the invasion growth rate of each species invading the other is positive following Chesson's criterion (Chesson 1982; Chesson et al. 1989). For this analysis we consider the virus as the IV subsystem (equation 23).

Fitness analysis in the coexistence regime

To assess the effect of adding the Infected class on fitness, we decompose in the coexistence regime the growth rate of the zooplankton and in this case of the free virus (equation 25), with or without fluctuations of their resources. The fluctuation free growth rate of predator P (either V or Z), *i.e.* when I and S concentrations are considered constant, is defined as follows:

$$\mu_P^0 = \mu_P(\bar{S}, \bar{I}), \tag{29}$$

where $\bar{S}$ and $\bar{I}$ are respectively the average concentration of S and I (over a periodic cycle in our case).
The nonlinearity in S (respectively, in I) is quantified as the difference between the average growth rate under fluctuating S (or I) and the growth rate at the average (*i.e.* fluctuation-free) values of S and I:

$$\epsilon_P^I = \overline{\mu_P}(\bar{S}, I) - \mu_P^0 \tag{30}$$

$$\epsilon_P^S = \overline{\mu_P}(S, \bar{I}) - \mu_P^0 \tag{31}$$

where $\overline{\mu_P}(\bar{S}, I)$ and $\overline{\mu_P}(S, \bar{I})$ are the average growth rate of P when S (respectively I) is constant and I (respectively S) is fluctuating.

Fourier analysis

To assess whether the system is stable or oscillating outside of transient dynamics, we performed a Fourier analysis of the virus time series in the last year of simulation (of 20 years). The fft function from the numpy Python library (Harris et al. 2020) is used and the frequency with the largest modulo is extracted. We consider the system to be a oscillating when the largest modulo is superior to 1.

Ecological metrics

We define the percentage of infected cells as follows:

$$\%I = 100.\frac{I}{P}, \tag{32}$$

where $P = S + I + R$ is the total phytoplankton concentration. The percentage of resistant cells (without considering infected cells) is:

$$\%R = 100.\frac{R}{S+R}. \tag{33}$$

We define the per-capita virus-induced mortality, m_V, and zooplankton-induced mortality, m_Z, as follows:

$$m_V = \frac{I}{P}.\frac{1}{\tau} \tag{34}$$

$$m_Z = g_Z.Z. \tag{35}$$

From these metrics, we define the percentage of virus-induced mortality:

$$\%V_m = 100.\frac{m_V}{m_V + m_Z + d_S}. \tag{36}$$

The net primary productivity at equilibrium is defined as the difference between photosynthesis and mortality of the phytoplankton (with contributions from susceptible and resistant cell classes):

$$NPP = ((\mu - d).S + (\mu.\zeta - d).R).\frac{106}{16}, \tag{37}$$

where the C:N Redfield ratio $\frac{106}{16}$ is used to convert into units of $\mu molC.d^{-1}.L^{-1}$.

Target concentrations and model error

We define target concentrations based on the values of virus and phytoplankton concentration measured in the field, generally measured in $individual.L^{-1}$ (Mojica et al. 2016; Leblanc et al. 2018; Carlson et al. 2022; Beckett et al. 2024) (including these targets in Table S4). For *Prochlorococcus*, the target concentration is defined as 10^8 $individual.L^{-1}$ (noted $ind.L^{-1}$ for any tracer throughout the text) in an oligotrophic environment and 2.10^8 $ind.L^{-1}$ in a mesotrophic environment, while its target concentration of phages are, respectively, 5.10^8 and 10^9 $ind.L^{-1}$ (Mojica et al. 2016; Carlson et al. 2022). For picoeukaryotes (based on picoeukaryote from Mojica et al. 2016) and a small diatom (based on concentrations of small diatoms from (Leblanc et al. 2018) and similar to concentration of nanoeukaryotes in Mojica et al. 2016), in a mesotrophic environment, target concentrations are respectively 2.10^7 and 2.10^6 $ind.L^{-1}$ (Mojica et al. 2016; Leblanc et al. 2018) and 2.10^7 and 10^9 $ind.L^{-1}$ for their respective viruses. We set the same target concentration for the diatom virus as the concentration for the *Prochlorococcus* phage as the diatom virus is of a similar size and diatom viruses can reach very high concentrations in culture experiments (Tomaru et al. 2021; Arsenieff et al. 2019). Finally, measured values of 1 to 10^5 $ind.L^{-1}$ for zooplankton are used (Schartau et al. 2010). We consider heterotrophic flagellates with a radius of 2.5 μm for cyanobacteria and a radius of 5 μm for the picoeukaryote and the small diatom (Schartau et al. 2010; Sherr et al. 1994). To further constrain the model outputs, we impose biologically realistic ranges for the percentage of infected cells (0.5% to 10%; Carlson et al. 2022) and the proportion of virus-induced mortality (0% to 50%). For diatoms, the upper bound on the percentage of infected cells is relaxed due to limited empirical constraints. These bounds are not included in the target concentration error metric (see below), but they must be satisfied during the optimization procedure. To assess the error between target concentrations and modeled concentrations for an environment e, we define the total absolute error, in %, as the sum of absolute relative errors across tracers:

$$D_e = \sum_{X=P,V,Z} \frac{|X_s^e - X_t^e|}{X_t^e}, \tag{38}$$

where X_s and X_t are respectively the theoretical and targeted concentrations of a tracer (P, V or Z). We define the average absolute error across environments (O oligotrophic, M mesotrophic) as a weighted mean across environments:

$$\overline{D} = \frac{1}{\sum_{e \in O,M} \alpha_e} \sum_{e \in O,M} \alpha_e . D_e. \tag{39}$$

For the picoeukaryote and the small diatom, a weight (parameter α_e) of 2 (*i.e.* it is counted twice) is given to the error in the mesotrophic environment as there exist no precise measurements of these organisms in oligotrophic environments (dominated by cyanobacteria) and target concentrations are more arbitrary.

Simulations and criterion of existence

Each model is simulated for 20 years using an integration time step of 30 minutes following the Runge-Kutta 4 integration scheme (Lotkin 1951) in a spatially implicit (no spatial dimension or 0D) setup. Simulations are run for a range of parameters values for each model, where we choose to provide particular focus on variations in the adsorption rate. For the $SIVZ$ and $SIVRZ$ models, which include an infected cell class, we also include assessment with respect to varying the latent period. The burst size is fixed by the life history trait model (see life history traits section). For the $SIVRZ$ model we also explore the adsorption rate and the resistance strength space while the latent period and burst size are fixed by the life history traits models. To operationally assess the final state of the model, we check whether the concentration of each tracer was found to be greater than 1 $ind.L^{-1}$ in the last year of simulation.

Results

Mechanisms of coexistence between the virus and the zooplankton

A trade-off between latent period and virulence facilitates coexistence

For the SVZ model of *Prochlorococcus* (Susceptible Phytoplankton–Virus–Zooplankton, Figure 1c; equation 2), which resembles a Lotka-Volterra system with one prey and two predators (Lotka 1920), coexistence occurs between the phytoplankton and either the virus or the zooplankton, but not both simultaneously. The outcome depends on the viral adsorption rate, with one predator excluding the other (Figure 2a). This aligns with the competitive exclusion principle (Armstrong et al. 1980), which states that two species competing for the same resource with linear growth rates cannot coexist indefinitely. For simplicity, we refer to the virus's adsorption rate (ϕ_S) multiplied by the probability of infection (ϵ) as its virulence throughout the remainder of the text. Operationally, we use the terms very, moderate, or mildly virulent to denote adsorption rates of $\phi_S > 10^{-9}$, $10^{-10} < \phi_S < 10^{-9}$, and $\phi_S < 10^{-10}$ $L.d^{-1}$ respectively.

To investigate mechanisms that may facilitate coexistence between the two predators, we introduce an infected class of phytoplankton (I) in the $SIVZ$ model (Figure 1d; equation 3). Introducing the infected class to the model adds a new parameter: the latent period of infection. Here we explore a parameter range for the latent period beyond measured maximum latent periods (maximum of 1.75 day in Edwards et al. 2018) and most likely beyond what is expected in the ocean, to assess the effect of this parameter across a large range and visualize transitions in model outputs. We find that the inclusion of the I class alone, regardless of whether it is grazed or not can facilitate coexistence between the virus and zooplankton. Virus-grazer coexistence is observed only when the carrying capacity term for the phytoplankton is retained and occurs within a narrow range of the viral latent period and adsorption rate (Figure 2e). Only moderate to very virulent viruses are able to coexist with the zooplankton in the region of the virulence spectrum where the virus excludes the grazer in the SVZ model (Figure 2a versus Figure 2e). As the virulence increases, the latent period required for the virus to persist also increases, reaching up to approximately 10 days for the most virulent viruses (much longer than the doubling time of the host, Figure 2e). These coexistence regimes are found to be unstable, generating limit cycles that are away from the equilibrium points of the system (Figure S5 and Figure S6a). This suggests a trade-off between the viral adsorption rate and latent period to facilitate coexistence, where sufficiently small oscillations are necessary to prevent the system from collapsing. The inclusion of the I class appears to have two opposing effects. First, in the case of coexistence, the time delay between the viral adsorption to the host and the burst of new viruses generates a limit cycle, with a short time shift between the peaks (highs and lows) of the virus and zooplankton population dynamics (Figure S5). These peaks may either follow one another in the same order (Figure S5a) or not (Figure S5b). Second, for very virulent viruses with a relatively short latent period, the time delay causes strong oscillations in the SIV dynamics, which can drive the system to extinction (Figure 2e), a behavior not seen in the SVZ model (Figure 2a). Interestingly, the inclusion of the I class can either support coexistence or lead to extinction, depending on the underlying ecological life-history traits.

To further investigate how the inclusion of the infected class (I) facilitates the coexistence regime, we performed an invasibility analysis following Chesson's mutual invasibility criterion of coexistence (Chesson 1982; Chesson et al. 1989). We find good agreement with mutual invasibility and the coexistence regime (Figure 3a,

b). However, the coexistence extends slightly further than Chesson's criterion validity range. For very virulent viruses with a long latent period, the SIV model collapses while there is coexistence for the $SIVZ$ model, suggesting a stabilizing effect of the zooplankton in this case. Following Modern Coexistence Theory (MCT, Ellner et al. 2019) the coexistence regime is also associated with a positive relative nonlinearity in S for the invasion growth rate of the zooplankton (Figure 3c). This suggests that this nonlinearity acts as the main mechanism of coexistence between the virus and the zooplankton. Nevertheless, this is not sufficient to ensure coexistence, as it is also positive or near 0 in the rest of the parameter space. Finally, we decompose the average growth rates of the free virus and the zooplankton in the coexistence regime with or without fluctuations of the I and S classes (Methods). We find that the fluctuation-free growth rate of the free virus, *i.e* considering the concentration of the I and S class to be constant (set as their mean), varies from near zero to extremely high values ($> 10^3\ d^{-1}$, Figure 3d). As expected from the formula of the free virus growth rate (equation 26), this result comes from a negative linear component in I for the growth rate of the free virus (Figure 3d). The inclusion of the infected class thus has a detrimental effect on the growth rate of the free virus, which, in turn, facilitates the coexistence. The lower clearance rate (g_Z) of the zooplankton compared to the infection rate of the virus ($\frac{\epsilon_V \cdot \phi_S}{Q_v}$, which is the viral clearance rate in the SVZ model) is effectively compensated by a reduced fitness of the free virus population due to the dynamics of the oscillating infected population. For the zooplankton, as expected from the linear growth rate of the latter, we observe no significant non linearities.

The inclusion of resistance facilitates coexistence through resource partitioning

An additional mechanism that may facilitate the coexistence of the virus and zooplankton is the introduction of a resistant type, which comes with an associated cost to its growth rate. This is represented by the $SVRZ$ model (Figure 1e, equation 4). In this model, we specifically consider extracellular resistance to viral infection, where the resistance is reflected by a reduced viral adsorption rate, denoted by the parameter ϕ_R (equations 4b and 4c). To explore this dynamic, we examine two scenarios: one where the resistant type exhibits partial resistance with a ratio of $\frac{\phi_S}{\phi_R} = 5$, and another where the resistance is complete, meaning $\phi_R = 0$ (fully resistant type).

For the partially resistant type, a coexistence regime is observed in the region characterized by viruses of moderate virulence (Figure 2i). In contrast, for the fully resistant type, this region extends into the domain characterized by very virulent viruses (Figure 2q). As anticipated, these coexistence regions are located within the part of the virulence spectrum where the virus excludes the grazer in the SVZ model (Figure 2a versus Figure 2i, q). Intuitively, the introduction of a resistant type decreases the virus's fitness, while allowing the zooplankton to graze on the resistant type, which experiences reduced susceptibility to viral effects. To illustrate this, we plot the dynamics of the $SVRZ$ model within the coexistence regime (Figure S7). Two distinct dynamic patterns emerge in this regime: either slowly dampened oscillations or sustained periodic oscillations. For a moderately virulent virus, the oscillations persist after 20 years of simulations, with the virus and the resistant type oscillating in opposite phases (Figure S7a, c). In the case of a slightly more virulent virus and a partially resistant type, the oscillations of the resistant type and the zooplankton dampen more quickly, while those of the susceptible type and the virus remain coupled (Figure S7b). Finally, for moderately virulent viruses, in the case of full resistance, we observe a stable equilibrium (Figure S7d). Importantly, adding the resistant type reduces the total virus abundance, and as viral virulence increases, the system transitions from dominance of the susceptible cell type to the resistant cell type. Overall, these results confirm that introducing a resistant type creates resource partitioning between the virus and the zooplankton, with the virus mainly targeting the susceptible type (though depending on the relative abudances of the S and R type), while the zooplankton consumes both types, primarily feeding on the more abundant one.

To further investigate this model, we set the latent period at 0.37 day ($\approx$ 9 h, based on the life history trait model) and examine the impact of resistance strength with a constant cost on the growth rate of the R type (Figure S8). As the virus virulence increases, the resistance strength required to achieve the coexistence state also increases (Figure S8a). Adding the infected class ($SIVRZ$ model, Figure 1f, equation 5) the state where the zooplankton is excluded now supports coexistence between the S and R types (Figure S8a versus S8e). Finally, we also test for an intracellular resistance model by modulating the probability of entering the infected state (parameter ϵ_{VR}). In this case, the coexistence state is reached at lower resistance strengths for very virulent viruses (Figure S8a, e versus S8i, m).

The inclusion of quadratic mortality terms for predators facilitates coexistence and stabilization

In ocean ecosystem models, quadratic mortality terms are used for grazers (Dutkiewicz et al. 2020) and have also been used for viruses (Talmy et al. 2019a; Beckett et al. 2024). For the zooplankton, the quadratic mortality represents top-down control by higher predators, assumed to scale with zooplankton density. For the virus, the quadratic mortality represents losses due to unspecific binding and collision with particulate matter. We find that the inclusion of a quadratic mortality term (Steele 1974) for the zooplankton in the SVZ model facilitates the coexistence regime in the adsorption rate region where the virus was previously excluded (Figure 2b versus 2a). In contrast, the inclusion of a quadratic mortality term for the virus facilitates coexistence in

the region where the zooplankton was previously excluded (Figure 2c versus 2a). The inclusion of both terms results in both regions entering the coexistence regime (Figure 2d). In the $SIVZ$, $SVRZ$ and $SIVRZ$ models, the effects are similar (Figure 2 and Figure S8). Notably, the inclusion of these higher-order loss terms also facilitates a coexistence state where the R type dominates, excluding the S type, for very virulent viruses and a partially resistant type (dark brown regions, Figure 2j, k, l, n, o, p). Interestingly, the region of R type dominance is larger for extracellular resistance than for intracellular resistance, suggesting that it might be more beneficial for invading a population and becoming dominant, assuming the same cost of resistance (Figure S8d, h versus S8l, p). Additionally, in the $S(I)VRZ$ models, the inclusion of the virus quadratic mortality extends the region where the S type dominates, excluding the R type (light brown region, Figure 2k, l, o, p, s, t, w, x). For the $S(I)VRZ$ model with a partially resistant type, as the virulence of the virus increases, there is a succession of coexistence states: first, the S type dominates (light brown region), then the S and R types coexist (gold brown region), and finally, the R type dominates (dark brown region, Figure 2l, p). It should be noted that the cases of S and R type dominance correspond to the same equilibrium. The only difference is the cost to the growth rate for the latter.

It is well known that quadratic mortality terms have a stabilizing effect (Poethke et al. 1987). To verify this in our system, we derive approximate model equilibria for the $SIVZ$ and $SIVRZ$ models in two cases: $d_{Z2} > 0$ with either $d_{V2} = 0$ or $d_{V2} > 0$ (see Supplementary Information for the mathematical derivations, equations S14-48, and Figure S9-11). We simulate the dynamics of the models and calculate the approximate theory (Methods) for four types of small phytoplankton: a small *Prochlorococcus*, a small *Synechococcus*, a picoeukaryote, and a small diatom (Table S1). We find a strong agreement between the approximate theory and the simulations ($SIVZ$, Figure S9 and $SIVRZ$, Figure S11), including system stability (shown in Figure S10 and S12), when compared to the Fourier analysis (Figure S6). The quadratic mortality terms strongly stabilize the system, with the viral quadratic mortality term acting to stabilize viral population dynamics for more virulent viruses. The oscillation dynamics is still maintained only for very virulent viruses and long latent periods (Figure S6). As expected from encounter rate theory (Huisman et al. 1999; Levin et al. 1977; Talmy et al. 2019b), the coexistence regime shifts toward more virulent viruses for larger organisms (Figure S9 and S11). The approximate theory is less accurate for larger organisms (diatoms), particularly for very virulent viruses in the $SIVZ$ model (Figure S9p) and for long latent periods in the $SIVRZ$ model, but it still effectively captures the coexistence regime (Figure S11p).

Toward the integration of viral lysis in ocean ecosystem models

The effect of including a virus: critical transitions and impact on the system

A crucial challenge in implementing viral lysis models in ocean ecosystem models is in assessing the viral impact on the ecosystem and identifying ecological parameter ranges that produce realistic concentrations of different biogeochemical tracers, as compared to field observations. To address this issue, we first analyze the dynamics of the models and the impact on the equilibria reached for a fixed latent period (Figure 4 for count concentrations and Figure S13 for nitrogen molar concentrations), determined by the life history trait model (Figure S3-4, Table S1). For all models we consider, mildly virulent viruses are excluded after approximately one year of simulation (Figure 4a, e, i, m). As the virulence of the virus increases, stable coexistence equilibria are first enabled by the addition of zooplankton quadratic mortality (Figure 4b), but these equilibria become unstable for more virulent viruses (Figure 4d, e). High virus count concentrations are reached in this case, generally much higher than the phytoplankton count concentration. Adding a viral quadratic mortality term strongly decreases the equilibrium virus concentration below the phytoplankton concentration (Figure 4f). As virulence increases, the virus concentration augments, leading to a decrease in phytoplankton concentration (Figure 4g), before the virus concentration decreases again for the very virulent viruses, accompanied by a sharp decline in phytoplankton concentration (Figure 4h). In the case of a partially resistant type, the same behavior is observed (Figure 4j, k), except for very virulent viruses, where the regime allows a new virus concentration peak where the resistant type dominates but the zooplankton is excluded (Figure 4l). For the fully resistant type (Figure 4m-p) coexistence with the zooplankton is maintained for very virulent viruses (Figure 4p).

To better understand these effects, we visualize the equilibrium concentrations of total phytoplankton, virus, and zooplankton (averaged over the last year in the case of oscillating dynamics) across the virulence spectrum and the latent period parameter space for the different models, including the quadratic mortality terms (Figure 5a-o). The total concentration of phytoplankton is significantly decreased by the presence of the virus only when the virus becomes sufficiently virulent, its encounter fitness (infection rate) surpassing that of the zooplankton (Figure 5a). The total phytoplankton concentration decreases from $\sim 10^{-1.2}$ to $10^{-3.1}$ $\mu molN.L^{-1}$ ($\sim 10^8$ to 10^6 $ind.L^{-1}$), slightly less than two orders of magnitude, for the most virulent viruses. Including a partially resistant cell type reduces this effect (decreasing to $\sim 10^{-2}$ $\mu molN.L^{-1}$ *i.e.* $\sim 10^{7.25}$ $ind.L^{-1}$), and the transitions between the three coexistence regimes (Figure 2p) become apparent (Figure 5b). In the case of the fully resistant type, the R type dominated regime is not reached (Figure 5c). Net primary productivity (NPP, Figure 5j-l) is directly related to phytoplankton concentration (equation 38, Figure 5a-c). Consequently, very virulent viruses have a dramatic decreasing effect on NPP (Figure 5j). Although we do not account for

the microbial loop in these models that has the potential to increase primary productivity, the resistance cost also decreases NPP (comparing the S type dominant regime to the mixed or R type dominant regimes, Figure 5k-l). The decomposition of the phytoplankton population into susceptible, infected, and resistant types, along with the percentage of resistant cells (relative to $S+R$), shows a rapid transition from a susceptible-dominated population to a resistant-dominated population as virulence increases (Figure S14g-p). The concentration of zooplankton is similarly affected (Figure 5g-i, decreasing from $\sim 10^{-1.3}$ to $10^{-2.3}$ $\mu molN.L^{-1}$ *i.e.* $\sim 10^{5.5}$ to $10^{4.5}$ $ind.L^{-1}$) and is excluded for the most virulent virus in the $SIVZ$ model (Figure 5g). For the virus, a relatively broad concentration peak is observed for moderately virulent viruses in the $SIVZ$ model (Figure 5e), which narrows in the $SIVRZ$ model as the resistant type takes over (Figure 5e-f), followed by a second peak in the case of the partially resistant type (Figure 5e). Particularly, the coexistence of the R and S types for very virulent viruses is enabled (full coexistence regime, Figure 2o). Surprisingly, in this case, the equilibrium viral concentration becomes independent of the latent period and is decreased (Figure 5e, f and the theoretical equilibria, equation 42-43). The quadratic mortality term used for the virus appears to be relatively high (Beckett et al. 2024), so the maximum concentrations reached are around $\sim 10^{-3.4}$ $\mu molN.L^{-1}$ *i.e.* $\sim 10^{8.5}$ $ind.L^{-1}$. Overall, increasing the latent period (τ) shifts the transitions between states towards more virulent viruses, with a modest effect for $\tau < 1$ day and a more pronounced effect as the latent period increases. Increasing τ also narrows the maximum viral concentration zone.

We next investigate the relative roles of the two predators in the system, along with the percentage of infections induced by the virus at equilibrium (Figure 4m-u). The zooplankton is generally more abundant in molar concentration than the virus, with a minimal molar ratio occurring at the maximum of free virus concentration (Figure 4m-o). For short latent periods ($\tau < 1$ day), the percentage of infected cells is generally low, transitioning from near 0 to 10% in the $SIVZ$ model as virulence increases (Figure 5p). For the $SIVRZ$ model, the highest percentages are found around the virus concentration peaks, although they remain very low (< 10 %) when the latent period is sufficiently low (Figure 5p-r). Increasing the latent period generally increases the percentages of infected cells, following a trade-off with the virulence of the virus (Figure 5p-r). More interestingly, the percentage of virus-induced mortality increases drastically with the virulence of the virus. For the $SIVZ$ model, it transitions from nearly 0% to $\sim$ 90% over $\sim$ 1.3 orders of magnitude in the virulence spectrum (Figure 5s), highlighting the strong sensitivity of the system to the virulence of the virus. This effect is primarily driven by the decrease in abundance of the zooplankton and does not necessarily imply a higher percentage of infected cells. Finally, adding the partially resistant type creates two peaks in the maximal percentage of virus-induced mortality (Figure 5t), while the fully resistant type results in a single peak (Figure 5u).

Bridging model and field ecology: models suggest the dominance of viral resistance

To assess the performance of each model against field measurements, we define concentration ranges and targets for total phytoplankton, viruses, and zooplankton, together with expected ranges for the percentage of infected cells and virus-induced mortality in two idealized epipelagic environments (Table S4; Mojica et al. 2016; Carlson et al. 2022; Schartau et al. 2010; Methods; Figure 6a). To illustrate the *in situ* measurements for *Prochlorococcus*, *Synechococcus*, their viruses and percentage of infected cells, we visualize distribution of their measurements from Carlson et al. 2022 in the North Pacific Subtropical Gyre (Figure S15). The measured concentrations in the literature were generally reported in $cell.L^{-1}$ and $virion.L^{-1}$ so we convert back to this unit for this analysis. Using the set of default parameters (Table S2), the $SIVZ$ model minimizes the distance to target concentrations in the mesotrophic environment for moderately virulent viruses near the maximum concentration of free virus (Figure 6b). Decomposing this distance among the different tracers shows that it is minimized around the peak concentration of free virus for all tracers, except for the zooplankton in the $SIVRZ$ model with the fully resistant type (Figure S16). For the $SIVRZ$ model with a partially resistant type, the minimum distance to the target concentrations is found in the regime dominated by the resistant type (Figure 6c). Conversely, the model with a fully resistant type shows poorer performance (Figure 6b). When the target concentration assumptions are relaxed, the entire coexistence regime falls within realistic concentration ranges for all models (Figure 6e-g). However, further constraining the output with the percentage of infected cells, virus-induced mortality, and a V/P ratio greater than 1 (Figure S17), a much narrower region of the virulence spectrum and latent period ecological parameter space aligns with observed empirical measurements (Figure 6h-j). These regions never encompass the coexistence regime including both the S and R types in abundance; instead, they occur in regions where only one type is dominant (Figure 2 versus Figure 6h-j).

Importantly, the "realistic" ecological parameter space is found within a virulence range with a lower adsorption rate, compared to a theoretical encounter model Talmy et al. 2019b, where the swimming speed is considered to have a multiplicative effect on diffusion (Figure 6h-j, equation 13, Methods). The $SIVRZ$ model with partial resistance represents the best match, as it minimizes the error to target concentrations close to the life-history trait model while also satisfying the other ecological constraints that we impose (Figure 6i). In general, these results suggest that including a level of extracellular resistance (compared to the encounter rate model) to the virus leads to a more accurate representation of the equilibrium achieved (Figure 6i).

To further test this hypothesis, we leverage the theoretical equilibria of the $SIVZ$ and $SIVRZ$ models

(Supplementary Information) to minimize model error in modeling target concentrations for both a mesotrophic and an oligotrophic environment (avoiding overfitting), across each of four considered types of phytoplankton: *Prochlorococcus*, *Synechococcus*, a picoeukaryote, and a small diatom (Table S4). The theoretical equilibria allow us to exhaustively explore a large ecological parameter space using a grid search approach. We choose to focus on the intracellular and extracellular resistance, the resistance cost, the linear and quadratic mortality of the virus (that can be null), and the quadratic mortality of the zooplankton (Table 1). We define the extracellular resistance as the ratio between the theoretical encounter rate and the fitted adsorption rate ($\frac{\phi_{th}}{\phi_R}$) while the intracellular resistance is defined as the inverse of the probability of infection ($\frac{1}{\epsilon_{VR}}$). Interestingly, we find that the optimal extracellular resistance is around $\sim 2-20$ for *Prochlorococcus*, *Synechococcus* and the picoeukaryote, while it is ~ 180 for a small diatom. Intracellular resistance factors were found to be in the same order of magnitude as extracellular resistance. Multiplying both types of resistance, we get resistances factor of 10, 60, 6 and 490 respectively for *Prochlorococcus*, *Synechococcus*, the picoeukaryote and the small diatom. Among the 200 best-fitting models, extracellular and intracellular resistance were significantly anticorrelated ($p < 0.001$) for *Prochlorococcus*, *Synechococcus*, and the small diatom, with correlation coefficients of $r = -0.76$, -0.81, and -0.24, respectively. The correlation was weak for the eukaryote (r = 0.11), but the best-fitting models exhibited a narrow range of extracellular resistance values. A resistance cost $(1-\zeta)$ of $\sim 0-0.2$ is found to be a good fit across organisms (except the diatom), although other parameters might also contribute to decreasing the growth rate in larger ocean models. The linear and quadratic mortality of the virus are also found to be lower compared to the default parameter. The quadratic mortlaity of the virus appeared relatively poorly constrained across the 200 best-fitting models for the four phytoplankton types. Finally, the best-fitting models suggest a largely higher quadratic mortality for the zooplankton compared to the default value used although the fitted range of the 200 best-fitting models remained wide.

We typically find low fitting errors in the differences between target and the modeled concentrations of the best fitting models (Table 2). However the modeled concentration of *Prochlorococcus* in the oligotrophic environment is 53 % higher than the target ($1.5.10^8$ $ind.L^{-1}$ instead of 10^8 $ind.L^{-1}$). This concentration remains within the range of measured *Prochlorococcus* concentration in the North Pacific Subtropical Gyre for which the mean (our target) is skewed due to a few low concentration measurements (Figure S15a). Including heterotrophic bacteria and their grazing by the same zooplankton might compensate this error. The picoeukaryote and diatom model performs well in both environments. Target virus concentrations are generally achieved. Generally, the percentages of infected cells reported by the models are small for cyanobacteria and the picoeukaryote (1.2 to 3.7% in the oligotrophic environment and 2.5 to 6.3% in the mesotrophic environment), which are in relative good agreement (slightly higher) compared to average field measurements (Carlson et al. 2022; Beckett et al. 2024 and Figure S13). They also correspond to a low percentage of virus-induced mortality between 0.3 and 0.5% in agreement with field measurements (Beckett et al. 2024). For the small diatom, the percentage of infected cells reaches 13% (most likely due to the the longer latent period) in the mesotrophic environment but still corresponds to a very low percentage of virus-induced mortality (0.27%).

Discussion

We proposed several models that incorporate viral lysis of phytoplankton designed for integration into large-scale ocean ecosystem models. Our approach transforms the SIV count model (Levin et al. 1977; Weitz 2015) into an elemental concentration SIV model that incorporates cellular and virion quota (Jover et al. 2014). Consequently, we explicitly wrote elemental fluxes equations linked to the viral "shunt" (Wilhelm et al. 1999) and the viral "shuttle" (Sullivan et al. 2017; Guidi et al. 2015; Zimmerman et al. 2020). This step is essential for integration into large-scale biogeochemical models, as it accounts for the distinct stoichiometry of viruses and their hosts, particularly their C:N:P ratios (Redfield 1934; Jover et al. 2014). As a result, viral lysis can significantly influence the composition of dissolved organic matter (DOM). Effects of virus on DOM has recently been demonstrated through the detection of cell wall debris (Heinrichs et al. 2022), alterations in DOM optical properties, changes in its bioavailability, and changes in heterotrophic bacterial community composition (Xiao et al. 2021). Viruses are an integral component of DOM, contributing significant proportions of their phosphorus content (exceeding 5% in certain environmental contexts), highlighting the substantial role of viruses in biogeochemical processes (Jover et al. 2014). Exploring the ecological and biogeochemical impacts of realistically encoded viruses within ecosystem models represents a next step in our research agenda.

To validate the feasibility of integrating viral lysis models into large-scale biogeochemical frameworks, we explored the mechanisms that could facilitate the coexistence of both a virus and a zooplankton preying on the same phytoplankton. Inclusion of the infected class (I) had a dual effect, either enabling limit cycles or driving the system to extinction through oscillatory dynamics. These oscillations in the infected class may play a crucial role in spatially resolved models by inducing out-of-equilibrium conditions, particularly in transition zones (Carlson et al. 2022). Next, the addition of a resistant type facilitated the coexistence of the two predators through niche partitioning. In particular, for the most virulent viruses, full resistance enabled the coexistence of both susceptible and resistant types, while partial resistance led to the exclusion of the susceptible type. The latter case (partial extracellular resistance) corresponds to the coexistence regime of a less virulent virus

and includes an eventual cost to the growth rate of the phytoplankton. The inclusion of this kind of resistant type in biogeochemical models, although it may be computationally costly, could lead to the system alternating between different coexistence regimes, with a potential decrease of primary productivity due to the resistance cost. The resistance cost may depend on the mutation (Bohannan et al. 2000; Chao et al. 1977) and follow trade-offs (Våge et al. 2013). In addition, the range of resistance, *i.e.* the resistance to multiple viruses, which we do not resolve here, can vary (Avrani et al. 2015). Importantly, natural populations might evolve to a reduced resistance range and favor maximal growth rates through compensatory mutations (Avrani et al. 2015). Finally, the inclusion of higher-order quadratic mortality terms for the predators expanded the coexistence regimes by stabilizing the system. Quadratic mortality terms also have a controlling role on the concentrations reached by the predators. These terms are not very well constrained and here we fitted values that are lower than those previously reported for viruses (Beckett et al. 2024) and higher than those used for zooplankton (Dutkiewicz et al. 2015a). Importantly, in large scale ecosystem models, other mechanisms of coexistence might be at play like currents and the size fractionation of zooplankton grazers (Dutkiewicz et al. 2020).

We then evaluated the impact of introducing the virus into the system, focusing on its effects on phytoplankton mortality and abundance, as well as its partitioning between the zooplankton and the virus. The outcomes were strongly influenced by the virulence of the virus: mild viruses had minimal impact, whereas highly virulent viruses induced substantial changes in the system's dynamics and equilibrium. As previously reported, a maximal concentration of free viruses was observed for mildly virulent strains, whereas the most virulent viruses were less abundant (Maidanik et al. 2022). This finding is consistent with field observations of cyanophages infecting *Prochlorococcus* populations in the global oceans (Maidanik et al. 2022). In addition, the system exhibited strong sensitivity, characterized by steep transitions in its ecological properties. In particular, we observed rapid shifts in the percentage of infected cells and virus-induced mortality across the virulence spectrum. The percentage of infected cells was predominantly influenced by the latent period, while virus-induced mortality showed a pronounced increase with higher viral adsorption rates. Thus, a high percentage of infected cells does not necessarily correspond to a high percentage of virus-induced mortality, and vice versa. Paradoxically, a highly virulent virus, despite its low abundance, can drive substantial phytoplankton mortality even when the percentage of infected cells at equilibrium is low. In the model, this phenomenon is driven primarily by the partial exclusion of zooplankton, which may, for instance, explain the negative correlations between viral and grazing rates observed in field studies (Biggs et al. 2021). These results further suggest that transient dynamics could readily emerge in spatially explicit models, potentially explaining the variability in ecological properties observed in the field, such as the percentage of infected cells and virus-induced mortality (Mojica et al. 2016; Biggs et al. 2021; Carlson et al. 2022; Beckett et al. 2024).

Finally, we compared the outputs of our models to field measurements of virus, phytoplankton, and zooplankton concentrations. Using the default ecological parameter set, the $SIVZ$ and $SIVRZ$ models performed similarly in minimizing the distance to target concentrations. However, the $SIVRZ$ model aligned more closely with the life history trait model describing the encounter rate between phytoplankton and their viruses. Notably and as expected (Weitz et al. 2015), this result suggests that incorporating resistance into the encounter rate model provides a better fit to empirical measurements. Furthermore, when fitting the model to target concentrations across a broad parameter range, we found the most appropriate extracellular resistance to be important, which we quantified here to range from a factor of 2 to 10 for the cyanobacteria and the picoeukaryote and 180 for the diatom compared to the biophysical encounter rate model. Interestingly, both extracellular resistance, directly affecting the adsorption rate and intracellular resistance, that decreased the probability of infection, were necessary to fit the models to field measurements. Anti-phage intracellular defense mechanisms are well-documented (Labrie et al. 2010; Avrani et al. 2015; Rousset et al. 2022), although some remain unidentified in marine cyanobacteria (Zborowsky et al. 2019). Notably, studies have shown that cyanophage resistance is predominantly extracellular against specialist phages, which target the most abundant high-light–adapted *Prochlorococcus* strains. In contrast, resistance is primarily intracellular against generalist phages, which infect the less abundant *Synechococcus* and low-light–adapted *Prochlorococcus* ecotypes (Zborowsky et al. 2019). These observations support our findings, suggesting that both types of resistance are important in marine phytoplankton. Future models may wish to include the potential for intracellular resistance to halt infections at various stages (Zborowsky et al. 2019). In our approach, we assumed that intracellular resistance reduced the probability of transitioning to the infected state. This could be further explored by modeling a transition rate from the infected class back to the susceptible class or by using more complex models that include intermediate infected states (Hinson et al. 2023; Dominguez-Mirazo et al. 2024).

Importantly, the encounter rate, and the adsorption rate, can be influenced by several factors not explored in our models. The encounter rate represents the biophysical maximum rate of interaction, while the adsorption rate reflects the actual rate of successful attachment, which is a fraction of the encounter rate. For instance, not all virions attach to their host upon encounter, as receptor heterogeneity on the cell surface (Murray et al. 1992; Talmy et al. 2019b) and cell surface properties (Yamada et al. 2023) can limit attachment. Furthermore, turbulent diffusion can either increase or decrease encounter rates depending on the turbulence intensity, with high turbulence potentially reducing encounter rates (Stocker 2012; Pecseli et al. 2014). Additionally, the adsorption rate might be decreased due to nonspecific binding to other particles in the environment, such as cellular debris

or other cells (Yamada et al. 2020), as well as through the formation of marine snow via the viral "shuttle" mechanism (Sullivan et al. 2017; Guidi et al. 2015; Zimmerman et al. 2020). This effect could be represented in a model as a Hill function inhibiting viral adsorption to the host (Igler 2022). Importantly, the magnitude of this effect may vary significantly in large-scale ocean models and in field conditions due to the pronounced heterogeneity of marine environments. These effects may not be as pronounced as the extracellular resistance proposed here, especially in oligotrophic and mesotrophic environments, such as those modeled here, which have low POM concentrations (Tanioka et al. 2022) but high dissolved organic matter (DOM) concentrations (Hansell et al. 2021). The extracellular resistance used here can thus be viewed as the cumulative effect of these limiting mechanisms in addition to biological resistance. Nevertheless, further research is needed to accurately account for and parameterize these effects for instance against time series data (Middleton et al. 2017).

Another limitation of our model is that it did not explicitly account for the microbial loop. This would require to explicitly include heterotrophic bacteria and inorganic nutrients in the model, which was done in another study (Weitz et al. 2015). Heterotrophic bacteria can remineralize dissolved organic nitrogen (DON) to dissolved inorganic nitrogen (DIN), thereby increasing nutrient availability to phototrophs, which is expected, in turn, to increase primary productivity (Fuhrman 1999; Wilhelm et al. 1999; Weitz et al. 2015). The system of ordinary differential equations we propose (equations 1a to 1c) and the fluxes to DON and PON (equation 1d and equation 1e) could be sufficient for integration of viral lysis into large-scale ocean ecosystem models. To fully close the model, one should redistribute mortality terms to the DIN, DON and PON compartments as done in Weitz et al. 2015. Future work will seek to couple models such as those we develop here into more complex ecosystem models.

Despite its relative simplicity, the $SIVRZ$ model, with a dominant R type, can effectively recapitulate the observed ecology of viral infections in oligotrophic and mesotrophic environments. By integrating algebraic theoretical results, field measurements, and life history trait models, we are able to accurately reproduce viral and phytoplankton concentrations, percentages of infected cells, and virus-induced mortality in both prokaryotic and eukaryotic phytoplankton. We characterized the effect of adding an infected class, which can have a dual impact on system stability, either stabilizing or destabilizing, depending on the trade-off between the latent period and the adsorption rate of the virus. In addition, the inclusion of the I class enables the model to accurately recapitulate the percentages of infected cells observed in the field. The percentage of infected cells in our model does not necessarily reflect the percentage of virus-induced mortality, as it depends on the virulence of the virus and whether it impacts the zooplankton. Finally, our models suggest that incorporating significant extracellular resistance into biophysical encounter rate models may be critical for accurately modeling viral lysis in large biogeochemical models, which is consistent with the measured resistance of phytoplankton strains (Zborowsky et al. 2019). Here we developed only one host-one virus models and did not account for viral (Gregory et al. 2019) and phytoplankton diversity (Dutkiewicz et al. 2020). The inclusion of multiple host-virus system is expected to increase phytoplankton coexistence (Thingstad 2000; Flynn et al. 2022). However, in a multiple one-host one-virus system it might be challenging to keep all virus-host pairs to fully coexist together (*i.e.* certain virus might be excluded and not others). We also used a very generic model of lytic viral infection. Other types of viral infection cycles exist, such as the lysogenic pathway (Tuttle et al. 2020), or for instance, in *G. huxleyi*, where virions are continuously produced by exocytosis (Homola et al. 2024).

In conclusion, integrating viral lysis in ocean ecosystem models may improve estimates of carbon cycling in the oceans and quantify the relative role of viruses and zooplankton in phytoplankton mortality. Importantly, the inclusion of viruses might also reduce the magnitude of discrepancies between models shown to to be linked to the parameterization of grazing (Rohr et al. 2023). We anticipate that the inclusion of viral lysis into large ecosystem models may also identify knowledge gaps and catalyze experimental and field-based studies to assess how viruses shape community ecology and biogeochemical cycles.

Code and data availability

All code and data necessary to generate all figures and tables are available at https://github.com/PaulFremont3/SIVZ_coexistence/ and are archived on Zenodo at https://doi.org/10.5281/zenodo.15866512 (Frémont 2025).

Acknowledgments

The authors acknowledge the University of Maryland supercomputing resources (http://hpcc.umd.edu) made available for conducting the research reported in this paper. This work is supported by grants from the Simons Foundation: no. 721231 to JSW, no. 549931 (Simons Collaboration on Computational Biogeochemical Modeling of Marine Ecosystems (CBIOMES)) and SFI-LS-Project-00011157 to SD and SFI-LS-Project-00010539 to DT. Paul Frémont is supported by a postdoctoral fellowship from the Simons Collaboration on Ocean Processes and Ecology (SCOPE), funded by the Simons Foundation through grants awarded to JSW. Stephen J. Beckett and Joshua S. Weitz are investigators at the University of Maryland-Institute for Health Computing, which is

supported by funding from Montgomery County, Maryland and The University of Maryland Strategic Partnership: MPowering the State, a formal collaboration between the University of Maryland, College Park and the University of Maryland, Baltimore. DT acknowledges NSF OCE grants no 2445508 and no 2023680. This is a contribution of the Simons Collaboration on Ocean Processes and Ecology (SCOPE). We thank members of the vDARWIN working group including Barbara Duckworth, Michael J. Follows, Oliver Jahn, Debbie Lindell and Daniel Muratore for constructive discussions and feedback.

Author Contributions

Conceptualization: PF, SJB, DD, JSW; methodology: PF; investigation: PF; code review: EC; writing—original draft: PF; writing—review & editing: PF, SJB, DD, CLF, DT, SD, JSW; funding acquisition: JSW, SD, DT.

Conflict of Interest Statement

Authors declare no competing interests.

References

Armstrong, Robert A. and Richard McGehee (1980). "Competitive Exclusion". In: *The American Naturalist* 115.2, pp. 151–170.

Arsenieff, L. et al. (2019). "First Viruses Infecting the Marine Diatom *Guinardia delicatula*". In: *Frontiers in Microbiology* 9, p. 3235.

Aumont, O. et al. (2015). "PISCES-v2: an ocean biogeochemical model for carbon and ecosystem studies". In: *Geoscientific Model Development* 8.8, pp. 2465–2513.

Avrani, Sarit and Debbie Lindell (Apr. 2015). "Convergent evolution toward an improved growth rate and a reduced resistance range in *Prochlorococcus* strains resistant to phage". In: *Proceedings of the National Academy of Sciences of the United States of America* 112.17, E2191–E2200.

Baudoux, Anne-Claire et al. (2007). "Viruses as mortality agents of picophytoplankton in the deep chlorophyll maximum layer during IRONAGES III". In: *Limnology and Oceanography* 52.6, pp. 2519–2529.

Beckett, Stephen J. et al. (2024). "Disentangling top-down drivers of mortality underlying diel population dynamics of Prochlorococcus in the North Pacific Subtropical Gyre". In: *Nature Communications* 15, p. 2105.

Berg, H.C. and E.M. Purcell (Nov. 1977). "Physics of chemoreception". In: *Biophysical Journal* 20.2, pp. 193–219.

Bergh, Ø. et al. (1989). "High abundance of viruses found in aquatic environments". In: *Nature* 340, pp. 467–468.

Biggs, T.E.G., J. Huisman, and C.P.D. Brussaard (2021). "Viral lysis modifies seasonal phytoplankton dynamics and carbon flow in the Southern Ocean". In: *The ISME Journal* 15, pp. 3615–3622.

Biswas, S et al. (Mar. 2020). "Modeling the avoidance behavior of zooplankton on phytoplankton infected by free viruses". In: *Journal of Biological Physics* 46.1, pp. 1–31.

Bohannan, B.J.M. and R.E. Lenski (2000). "Linking genetic change to community evolution: insights from studies of bacteria and bacteriophage". In: *Ecology Letters* 3.4, pp. 362–377.

Breiman, L. and A. Cutler (2012). *randomForest: Breiman and Cutler's Random Forests for Classification and Regression*. https://www.stat.berkeley.edu/~breiman/RandomForests/. R package version 4.1.0.

Carlson, Michael C. G., François Ribalet, Ilana Maidanik, et al. (2022). "Viruses affect picocyanobacterial abundance and biogeography in the North Pacific Ocean". In: *Nature Microbiology* 7, pp. 570–580.

Chao, Lin, Bruce R. Levin, and Frank M. Stewart (Mar. 1977). "A Complex Community in a Simple Habitat: An Experimental Study with Bacteria and Phage". In: *Ecology* 58.2, pp. 369–378.

Chesson (1982). "The stabilizing effect of a random environment". In: *Journal of Mathematical Biology* 15, pp. 1–36.

Chesson and Ellner (1989). "Invasibility and stochastic boundedness in monotonic competition models". In: *Journal of Mathematical Biology* 27, pp. 117–138.

Chesson, Peter (2000). "Mechanisms of Maintenance of Species Diversity". In: *Annual Review of Ecology and Systematics* 31, pp. 343–366.

Demory, David et al. (2020). "Linking Light-Dependent Life History Traits with Population Dynamics for ¡i¿Prochlorococcus¡/i¿ and Cyanophage". In: *mSystems* 5.2.

Demory, David et al. (2021). "A thermal trade-off between viral production and degradation drives virus-phytoplankton population dynamics". In: *Ecology Letters* 24.6, pp. 1133–1144.

Dominguez-Mirazo, Marian et al. (2024). "Accounting for cellular-level variation in lysis: implications for virus–host dynamics". In: *mBio*, e01376–24.

Dunne, Jennifer A. et al. (2013). "Parasites Affect Food Web Structure Primarily through Increased Diversity and Complexity". In: *PLoS Biology* 11.6, e1001579.

Dussart, B. M. (1965). “Les differentes categories de plancton”. In: *Hydrobiologia* 26, pp. 72–74.
Dutkiewicz, S. et al. (2015a). “Impact of ocean acidification on the structure of future phytoplankton communities”. In: *Nature Climate Change* 5, pp. 1002–1006.
Dutkiewicz, S. et al. (2020). “Dimensions of marine phytoplankton diversity”. In: *Biogeosciences* 17.3, pp. 609–634.
Dutkiewicz, Stephanie et al. (2015b). “Capturing optically important constituents and properties in a marine biogeochemical and ecosystem model”. In: *Biogeosciences* 12, pp. 4447–4481.
Edwards, KF and GF Steward (May 2018). “Host Traits Drive Viral Life Histories across Phytoplankton Viruses”. In: *The American Naturalist* 191.5, pp. 566–581.
Edwards, KF, GF Steward, and CR Schvarcz (Feb. 2021). “Making sense of virus size and the tradeoffs shaping viral fitness”. In: *Ecology Letters* 24.2, pp. 363–373.
Einstein, A. (1905). “Über die von der molekularkinetischen Theorie der Wärme geforderte Bewegung von in ruhenden Flüssigkeiten suspendierten Teilchen”. In: *Annalen der Physik* 322.8, pp. 549–560.
Ellner et al. (2019). “An expanded modern coexistence theory for empirical applications”. In: *Ecology Letters* 22.1, pp. 3–18.
Eppley, Richard W. and Bruce J. Peterson (1979). “Particulate organic matter flux and planktonic new production in the deep ocean”. In: *Nature* 282, pp. 677–680.
Field, Christopher B. et al. (1998). “Primary Production of the Biosphere: Integrating Terrestrial and Oceanic Components”. In: *Science* 281.5374, pp. 237–240.
Flynn, Kevin J. et al. (2022). “‘Boom-and-busted’ dynamics of phytoplankton–virus interactions explain the paradox of the plankton”. In: *New Phytologist* 234.4, pp. 1348–1360.
Frémont, Paul (2025). *SIVZ_coexistence*. Version v1.0. Zenodo archive, https://doi.org/10.5281/zenodo.15866512.
Frémont, Paul et al. (2022). “Restructuring of plankton genomic biogeography in the surface ocean under climate change”. In: *Nature Climate Change* 12, pp. 393–401.
Fuhrman, J.A. (1999). “Marine viruses and their biogeochemical and ecological effects”. In: *Nature* 399, pp. 541–548.
Fuhrman, Jed A. and Rachel T. Noble (1995). “Viruses and protists cause similar bacterial mortality in coastal seawater”. In: *Limnology and Oceanography* 40.7, pp. 1236–1242.
Gause, G. F. (1934). *The Struggle for Existence*. Baltimore: Williams and Wilkins.
Gregory, A.C. et al. (2019). “Marine DNA Viral Macro- and Microdiversity from Pole to Pole”. In: *Cell* 177.5, 1109–1123.e14.
Guidi, Lionel et al. (2015). “Plankton networks driving carbon export in the oligotrophic ocean”. In: *Nature* 532, pp. 465–470.
Hansell, D. A. and M. V. Orellana (2021). “Dissolved Organic Matter in the Global Ocean: A Primer”. In: *Gels* 7.3, p. 128.
Hardin, Garrett (1960). “The Competitive Exclusion Principle”. In: *Science*. New Series 131.3409, pp. 1292–1297.
Harris, Charles R. et al. (Sept. 2020). “Array programming with NumPy”. In: *Nature* 585.7825, pp. 357–362.
Hastie, Trevor, Robert Tibshirani, and Jerome Friedman (2009). *The Elements of Statistical Learning. Data Mining, Inference, and Prediction, Second Edition*. Springer New York, NY.
Heinrichs, Mara E. et al. (May 2022). “Deciphering the Virus Signal Within the Marine Dissolved Organic Matter Pool”. In: *Frontiers in Microbiology* 13. Section: Aquatic Microbiology.
Henson, Stephanie A., Richard Sanders, and Esben Madsen (2012). “Global patterns in efficiency of particulate organic carbon export and transfer to the deep ocean”. In: *Global Biogeochemical Cycles* 26.1.
Hin, Vincent et al. (Dec. 2011). “Coexistence of predator and prey in intraguild predation systems with ontogenetic niche shifts”. In: *The American Naturalist* 178.6, pp. 701–714.
Hinson, A. et al. (2023). “A model of algal-virus population dynamics reveals underlying controls on material transfer”. In: *Limnology and Oceanography* 68, pp. 165–180.
Holt, Robert D. and Gary A. Polis (1997). “A Theoretical Framework for Intraguild Predation”. In: *The American Naturalist* 149.4, pp. 745–764.
Homola, Miroslav et al. (2024). “Structure and Replication Cycle of a Virus Infecting Climate-Modulating Alga Emiliania huxleyi”. In: *Science Advances* 10, eadk1954.
Huisman, Jef and Franz J. Weissing (1999). “Biodiversity of plankton by species oscillations and chaos”. In: *Nature* 402.6760, pp. 407–410.
Igler, Claudia (2022). “Phenotypic flux: The role of physiology in explaining the conundrum of bacterial persistence amid phage attack”. In: *Virus Evolution* 8.2.
Ilyina, T. et al. (2013). “Global ocean biogeochemistry model HAMOCC: Model architecture and performance as component of the MPI-Earth system model in different CMIP5 experimental realizations”. In: *Journal of Advances in Modeling Earth Systems* 5, pp. 287–315.
Jover, L. et al. (2014). “The elemental composition of virus particles: implications for marine biogeochemical cycles”. In: *Nature Reviews Microbiology* 12, pp. 519–528.

Kiørboe, Thomas (2011). “How zooplankton feed: mechanisms, traits and trade-offs”. In: *Biological Reviews* 86.2, pp. 311–339.

Laber, C. P. et al. (2018). “Coccolithovirus facilitation of carbon export in the North Atlantic”. In: *Nature Microbiology* 3, pp. 537–547.

Labrie, S. J., J. E. Samson, and S. Moineau (2010). “Bacteriophage resistance mechanisms”. In: *Nature Reviews Microbiology* 8.5. Epub 2010 Mar 29, pp. 317–327.

Leblanc, K., B. Quéguiner, F. Diaz, et al. (2018). “Nanoplanktonic diatoms are globally overlooked but play a role in spring blooms and carbon export”. In: *Nature Communications* 9.1, p. 953.

Levin, Bruce R., Frank M. Stewart, and Lin Chao (1977). “Resource-Limited Growth, Competition, and Predation: A Model and Experimental Studies with Bacteria and Bacteriophage”. In: *The American Naturalist* 111.977, pp. 3–24.

Lotka, Alfred J. (1920). “Analytical Note on Certain Rhythmic Relations in Organic Systems”. In: *Proceedings of the National Academy of Sciences* 6.7, pp. 410–415.

Lotkin, Max (1951). “On the Accuracy of Runge-Kutta’s Method”. In: *Mathematical Tables and Other Aids to Computation* 5.35, pp. 128–133.

Maidanik, I. et al. (Sept. 2022). “Cyanophages from a less virulent clade dominate over their sister clade in global oceans”. In: *The ISME Journal* 16.9. Epub 2022 Jun 20. PMID: 35726021; PMCID: PMC9381782, pp. 2169–2180.

Mateus, M.D. (2017). “Bridging the gap between knowing and modeling viruses in marine systems - An upcoming frontier”. In: *Frontiers in Marine Science* 3.

Menden-Deuer, Susanne and Evelyn J. Lessard (2000). “Carbon to volume relationships for dinoflagellates, diatoms, and other protist plankton”. In: *Limnology and Oceanography* 45.3, pp. 569–579.

Middleton, Julia E. et al. (2017). “Functional dynamics of *Emiliania huxleyi* virus–host interactions across multiple spatial scales”. In: *Limnology and Oceanography* 62.2, pp. 757–765.

Mojica, K.D.A. et al. (2016). “Latitudinal variation in virus-induced mortality of phytoplankton across the North Atlantic Ocean”. In: *The ISME Journal* 10, pp. 500–513.

Mruwat, N. et al. (2021). “A single-cell polony method reveals low levels of infected Prochlorococcus in oligotrophic waters despite high cyanophage abundances”. In: *The ISME Journal* 15, pp. 41–54.

Murray, Ag and Gardner H. Jackson (1992). “Viral dynamics: a model of the effects of size shape, motion and abundance of single-celled planktonic organisms and other particles”. In: *Marine Ecology Progress Series* 89, pp. 103–116.

Negrete-García, Gabriela et al. (2022). “Plankton energy flows using a global size-structured and trait-based model”. In: *Progress in Oceanography* 209, p. 102898.

Orr, James A., David W. Armitage, and Andrew D. Letten (2025). “Coexistence Theory for Microbial Ecology, and Vice Versa”. In: *Environmental Microbiology.*

Pecseli, H. L., J. K. Trulsen, and Ø. Fiksen (2014). “Predator – prey encounter and capture rates in turbulent environments”. In: *Limnology and Oceanography: Fluids and Environments* 4, pp. 85–105.

Poethke, H. J. and M. Kirchberg (1987). “On the stabilizing effect of density-dependent mortality factors”. In: *Oecologia* 74.1, pp. 156–158.

Polis, Gary A. and Robert D. Holt (May 1992). “Intraguild predation: The dynamics of complex trophic interactions”. In: *Trends in Ecology & Evolution* 7.5, pp. 151–154.

Proctor, L. and J. A. Fuhrman (1990). “Viral mortality of marine bacteria and cyanobacteria”. In: *Nature* 343, pp. 60–62.

Redfield, Alfred C. (1934). “On the Proportions of Organic Derivatives in Sea Water and their Relation to the Composition of Plankton”. In: *James Johnstone Memorial Volume*, pp. 177–192.

Rohr, T. et al. (2023). “Zooplankton grazing is the largest source of uncertainty for marine carbon cycling in CMIP6 models”. In: *Communications Earth & Environment* 4, p. 212.

Rousset, F. et al. (2022). “Phages and their satellites encode hotspots of antiviral systems”. In: *Cell Host & Microbe* 30.5, 740–753.e5.

Schartau, Markus, Michael R. Landry, and Robert A. Armstrong (Aug. 2010). “Density estimation of plankton size spectra: a reanalysis of IronEx II data”. In: *Journal of Plankton Research* 32.8, pp. 1167–1184.

Séférian, R. et al. (2020). “Tracking Improvement in Simulated Marine Biogeochemistry Between CMIP5 and CMIP6”. In: *Current Climate Change Reports* 6, pp. 95–119.

Sherr, E. B. and B. F. Sherr (1994). “Bacterivory and herbivory: Key roles of phagotrophic protists in pelagic food webs”. In: *Microbial Ecology* 28.2, pp. 223–235.

Sieben, Andrew J., Joseph R. Mihaljevic, and Lauren G. Shoemaker (2022). “Quantifying mechanisms of coexistence in disease ecology”. In: *Ecology* 103.12, e3819.

Steele, John H. (1974). *The Structure of Marine Ecosystems.* Harvard University Press, p. 144.

Stock, Charles A. et al. (2020). “Ocean Biogeochemistry in GFDL’s Earth System Model 4.1 and Its Response to Increasing Atmospheric CO_2”. In: *Journal of Advances in Modeling Earth Systems* 12.

Stocker, R. (2012). “Marine microbes see a sea of gradients”. In: *Science* 338, pp. 628–633.

Straile, Dietmar (1997). “Gross growth efficiencies of protozoan and metazoan zooplankton and their dependence on food concentration, predator-prey weight ratio, and taxonomic group”. In: *Limnology and Oceanography* 42.6, pp. 1375–1385.

Sullivan, Matthew B., Joshua S. Weitz, and Steven Wilhelm (2017). “Viral ecology comes of age”. In: *Environmental Microbiology Reports* 9.1, pp. 33–35.

Suttle, Curtis A. (2007). “Marine viruses — major players in the global ecosystem”. In: *Nature Reviews Microbiology* 5, pp. 801–812.

Tagliabue, Alessandro et al. (2016). “How well do global ocean biogeochemistry models simulate dissolved iron distributions?” In: *Global Biogeochemical Cycles* 30.2, pp. 149–174.

Talmy, David et al. (2019a). “An empirical model of carbon flow through marine viruses and microzooplankton grazers”. In: *Environmental Microbiology* 21.6, pp. 2171–2181.

Talmy, David et al. (2019b). “Contrasting Controls on Microzooplankton Grazing and Viral Infection of Microbial Prey”. In: *Frontiers in Marine Science* 6.

Tanioka, T., A.A. Larkin, A.R. Moreno, et al. (2022). “Global Ocean Particulate Organic Phosphorus, Carbon, Oxygen for Respiration, and Nitrogen (GO-POPCORN)”. In: *Scientific Data* 9, p. 688.

Thingstad, T. F. and S. Våge (2019). “Host–virus–predator coexistence in a grey-box model with dynamic optimization of host fitness”. In: *ISME Journal* 13, pp. 3102–3111.

Thingstad, T. Frede (2000). “Elements of a theory for the mechanisms controlling abundance, diversity, and biogeochemical role of lytic bacterial viruses in aquatic systems”. In: *Limnology and Oceanography* 45.6, pp. 1320–1328.

Tomaru, Y., H. Yamaguchi, and T. Miki (2021). “Growth Rate-dependent Cell Death of Diatoms due to Viral Infection and Their Subsequent Coexistence in a Semi-continuous Culture System”. In: *Microbes and Environments* 36.1, ME20116.

Tuttle, Matthew J. and Alison Buchan (Dec. 2020). “Lysogeny in the oceans: Lessons from cultivated model systems and a reanalysis of its prevalence”. In: *Environmental Microbiology* 22.12. Epub 2020 Sep 29, pp. 4919–4933.

Våge, S., J. E. Storesund, and T. F. Thingstad (June 2013). “Adding a cost of resistance description extends the ability of virus-host model to explain observed patterns in structure and function of pelagic microbial communities”. In: *Environmental Microbiology* 15.6, pp. 1842–1852.

Venables, W. N. and B. D. Ripley (2002). *Modern Applied Statistics with S*. 4th. New York: Springer.

Verity, Peter G. et al. (1992). “Relationships between cell volume and the carbon and nitrogen content of marine photosynthetic nanoplankton”. In: *Limnology and Oceanography* 37.7, pp. 1434–1446.

Weitz, Joshua S. (2015). *Quantitative Viral Ecology: Dynamics of Viruses and Their Microbial Hosts*. Princeton, NY: Princeton University Press.

Weitz, Joshua S. et al. (2015). “A multitrophic model to quantify the effects of marine viruses on microbial food webs and ecosystem processes”. In: *The ISME Journal* 9, pp. 1352–1364.

Wigington, Charles H. et al. (2016). “Re-examination of the relationship between marine virus and microbial cell abundances”. In: *Nature Microbiology* 1, p. 15024.

Wilhelm, Steven W. and Curtis A. Suttle (Oct. 1999). “Viruses and Nutrient Cycles in the Sea: Viruses play critical roles in the structure and function of aquatic food webs”. In: *BioScience* 49.10, pp. 781–788.

Wood, S. N. (2004). “Stable and Efficient Multiple Smoothing Parameter Estimation for Generalized Additive Models”. In: *Journal of the American Statistical Association*.

Xiao, Xilin et al. (Jan. 2021). “Viral Lysis Alters the Optical Properties and Biological Availability of Dissolved Organic Matter Derived from *Prochlorococcus* Picocyanobacteria”. In: *Microbial Ecology*. Research Article.

Yamada, Y. et al. (2018). “Aggregate formation during the viral lysis of a marine diatom”. In: *Frontiers in Marine Science* 5.

Yamada, Y. et al. (2020). “Viral Attachment to Biotic and Abiotic Surfaces in Seawater”. In: *Applied and Environmental Microbiology* 86.3, e01687–19.

Yamada, Yosuke et al. (2023). “Bacterial surface roughness regulates nanoparticle scavenging in seawater”. In: *Limnology and Oceanography* 68.5, pp. 1142–1153.

Yamamichi, Masato, Theo Gibbs, and Jonathan M. Levine (Aug. 2022). “Integrating eco-evolutionary dynamics and modern coexistence theory”. In: *Ecology Letters*.

Zakem, Emily J., Ahmed Al-Haj, Matthew J. Church, et al. (2018). “Ecological control of nitrite in the upper ocean”. In: *Nature Communications* 9, p. 1206.

Zborowsky, Sophia and Debbie Lindell (2019). “Resistance in marine cyanobacteria differs against specialist and generalist cyanophages”. In: *Proceedings of the National Academy of Sciences* 116.34, pp. 16899–16908.

Zimmerman, Addison E. et al. (2020). “Metabolic and biogeochemical consequences of viral infection in aquatic ecosystems”. In: *Nature Reviews Microbiology* 18, pp. 21–34.

Zwirglmaier, Katrin et al. (2009). “Differential grazing of two heterotrophic nanoflagellates on marine Synechococcus strains”. In: *Environmental Microbiology* 11.7, pp. 1767–1776.

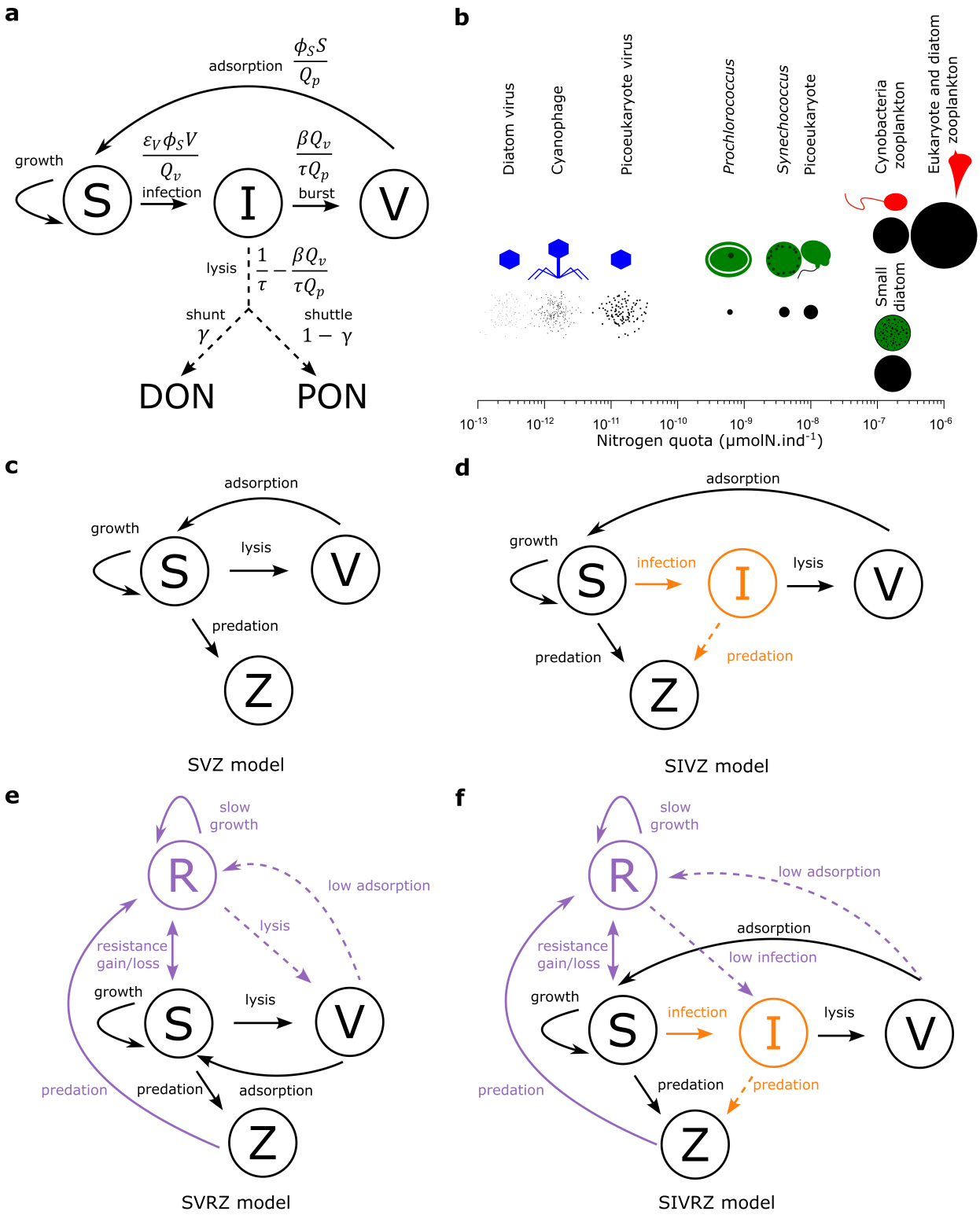

Figure 1 | Model sketches. (**a**) Model sketch of the SIV elemental concentration model including a shunt and a shuttle term represented respectively as a flux (dashed arrows, not explicitly simulated) to the dissolved organic nitrogen (DON) and the particulate organic nitrogen pool (PON). DON and PON are not represented as explicit compartments here as we did not model their full dynamics. A fraction γ (respectively $1-\gamma$) of the lysate is "shunted" ("shuttled") to DON (to PON). The rates of matter fluxes (in d^{-1}) are presented for each arrow linked to the inclusion of the viral lysis component (except for the viral decay term and the unsuccessful infection term). (**b**) Nitrogen molar quotas of the different phytoplankton, their respective virus and grazer used in this study. Under the representation of each organism, the radius of each black circle is proportional to the cube root of the nitrogen molar quota, reflecting the scaleing og nitrogen with cell volume. Each virus is shown 100 times for better visibility. The picoeukaryote morphology is inspired from *Micromonas pusilla* and the small diatom from *Minidiscus comicus*. Zooplankton are represented by a heterotrophic nanoflagellate for cyanobacteria grazing and by a heterotrophic dinoflagellate for eukaryotic phytoplankton grazing. Sketches of the different viral infection models used in the study: (**c**) SVZ model. (**d**) $SVRZ$ model. (**e**) $SIVZ$ model. (**f**) $SIVRZ$ model . S: Susceptible, I: Infected, V: Virus, Z: Zooplankton, R: Resistant type. Arrows represent fluxes of matter. Dashed arrows (**c-d**) represent optional terms. Orange and purple color respectively indicate fluxes linked to the addition of the I and R type.

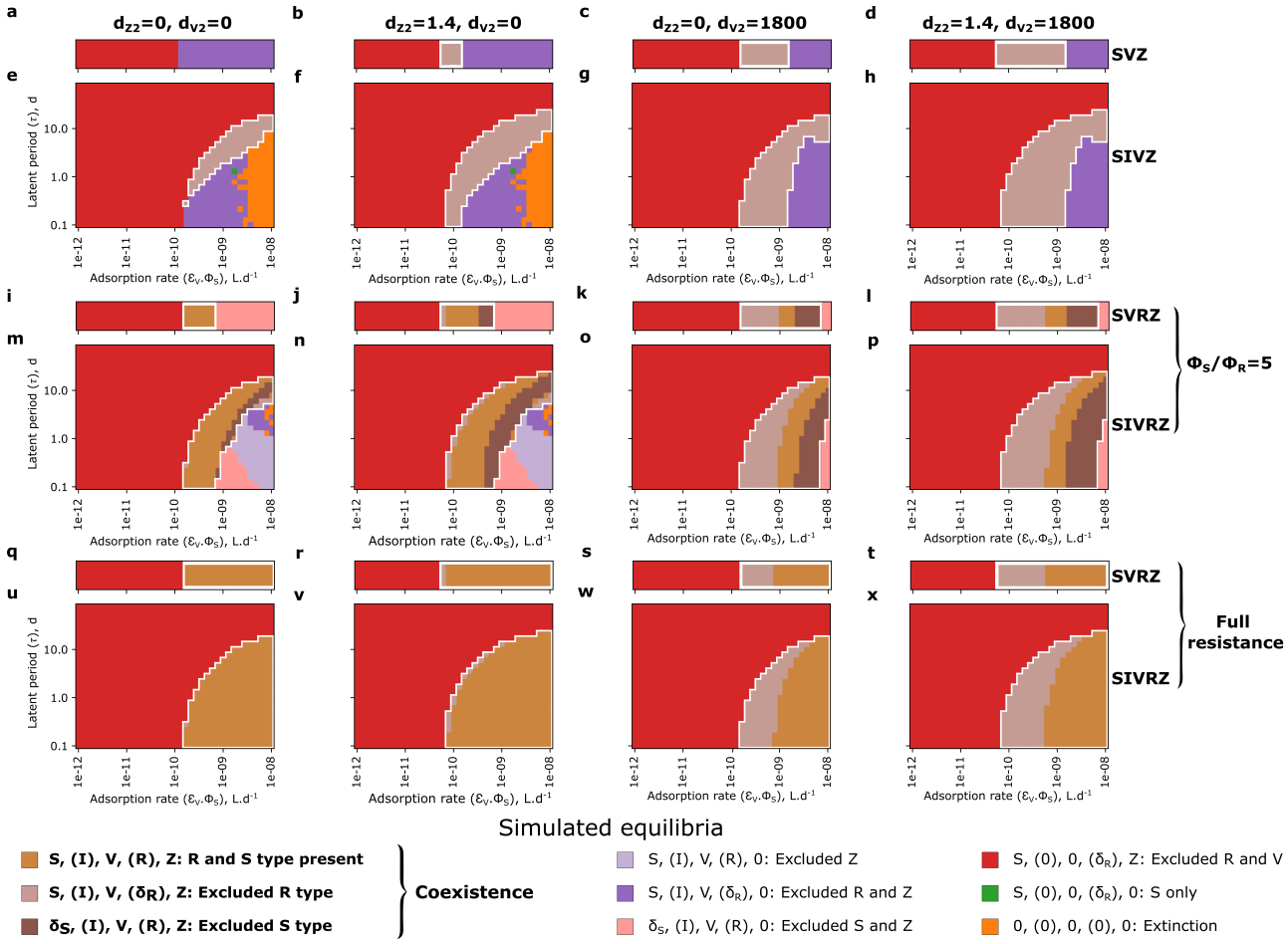

Figure 2 | Approximate simulated equilibrium regimes of a virus and a zooplankton modeled as predators of a *Prochlorococcus* for different types of viral lysis models across the adsorption rate and the latent period parameter space. (**a-d**) SVZ model. (**e-h**) SVZ model. (**i-l**) Extracellular $SVRZ$ model with a partially resistant type: $\frac{\phi_S}{\phi_R} = 10$. (**m-p**) Extracellular $SIVRZ$ model with a partially resistant type: $\frac{\phi_S}{\phi_R} = 10$. (**q-t**) Extracellular $SVRZ$ model with a fully resistant type. (**u-x**) Extracellular $SIVRZ$ model with a fully resistant type. From left to right panels: quadratic mortality terms respectively absent, present for the zooplankton only, present for the virus only, and present for both the zooplankton and the virus. The quadratic mortality terms are in $(\mu molN.L^{-1}).d^{-1}$. The SVZ model was run 25 years to allow full exclusion while the other models were run for 20 years. In the latter case, the equilibrium might not be reached yet. In addition some numerical instabilities might explain the fuzzy transitions between regions with different regimes. To define the equilibrium reached in each simulation we test whether each tracer had a concentration superior to 1 $ind.L^{-1}$ in the last yera of simulation. For each panel, the white contour denotes the coexistence regime.

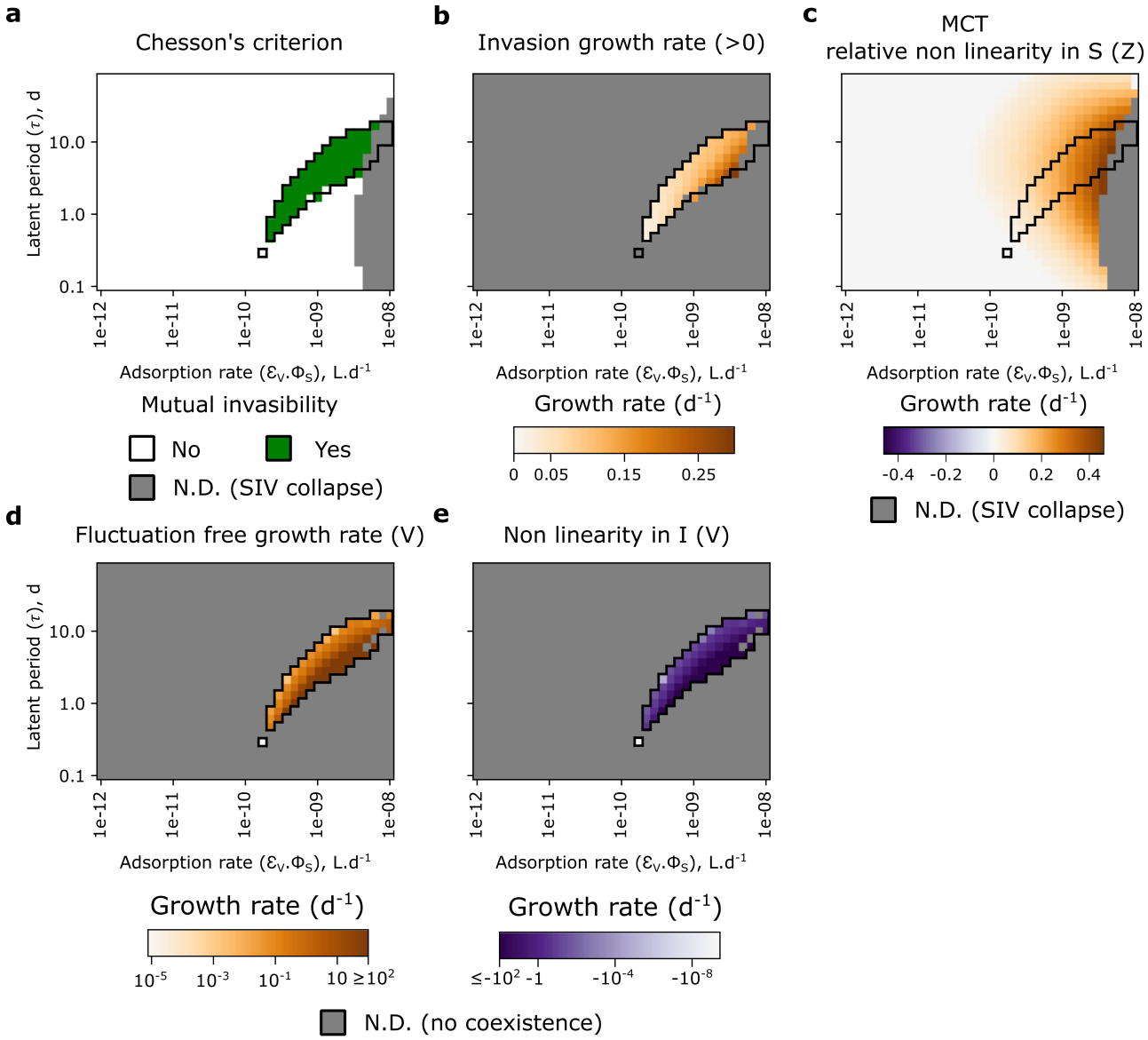

Figure 3 | Mechanisms facilitating coexistence of the $SIVZ$ model with the inclusion of the infected class. (**a**) Chesson's criterion of mutual invasibility. In the grey area, the analysis is not possible as the SIV model collapses in this region. (**b**) Total invasion growth rate (virus + zooplankton) when the Chesson's criterion is valid. (**c**) Relative nonlinearity in S for the zooplankton using Modern Coexistence Theory (MCT). (**d**) Fluctuation free growth rate of the free virus in the case of coexistence. (**e**) Nonlinearity in I in the case of coexistence: the growth rate of the free virus is decreased due to the non linear oscillations of the I class. For each panel, the contour of the regime reached by the the $SIVZ$ model after 20 years of simulations, without quadratic mortality terms for the predators, is presented as a black contour. N.D.: Not defined.

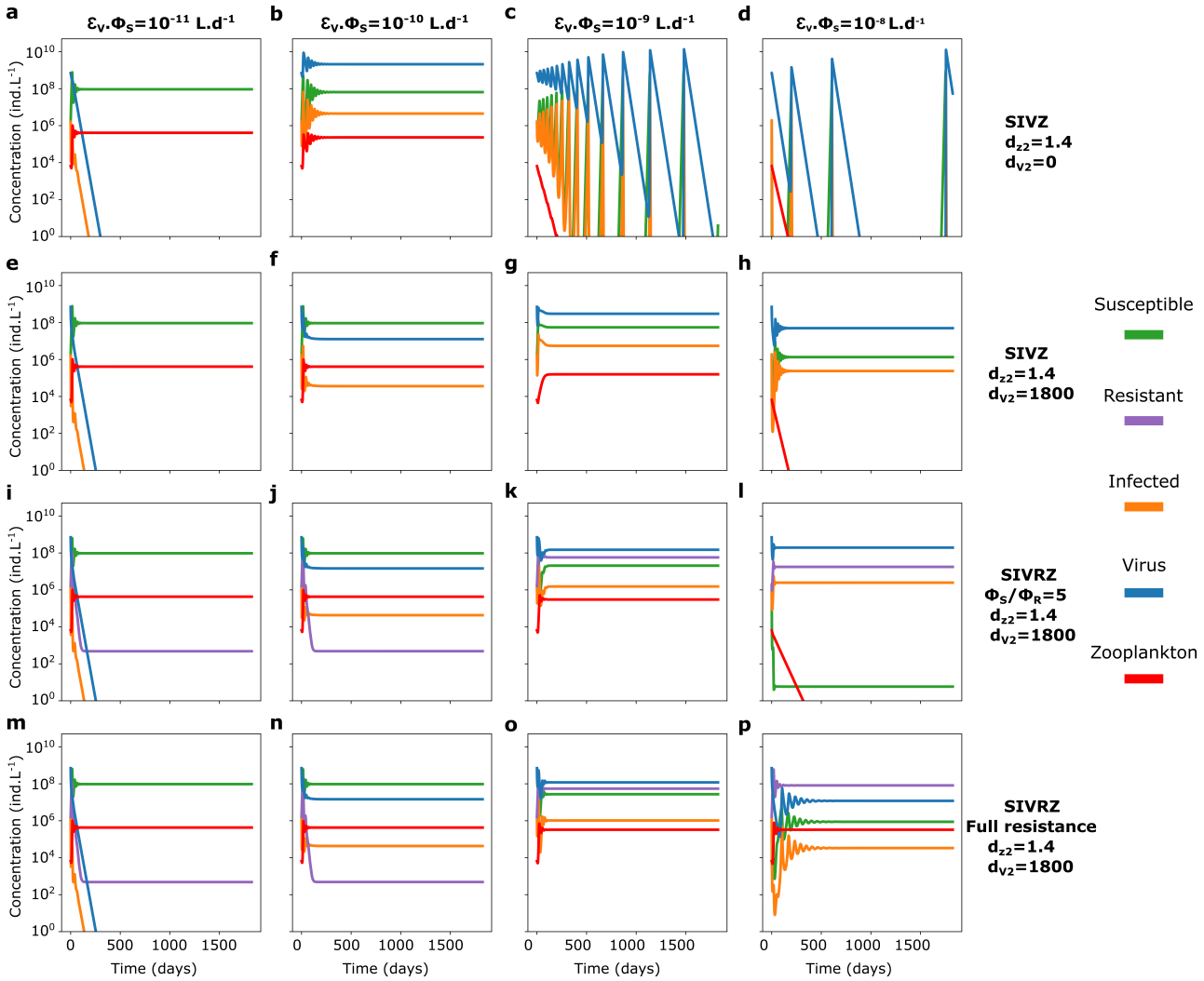

Figure 4 | Five year time series of the $SIVZ$ and the extracellular $SIVRZ$ models for *Prochlorococcus* for four different adsorption rates of the virus and different resistant type strength. Adsorption rate from $\epsilon_V.\phi_S = 10^{-11}\ L.d^{-1}$ to $\epsilon_V.\phi_S = 10^{-8}\ L.d^{-1}$ ($\epsilon_V = 1$) for the $SIVZ$ model (**a-d**) without and (**e-h**) with the quadratic mortality term of the virus, for the $SIVRZ$ model (**i-l**) with a partially resistant type and (**m-p**) a fully resistant type, both with the quadratic mortality term of the virus. The tracers' molar concentrations were converted in count concentrations using the cellular and virion quotas (see Figure S13 for time series in molar concentrations). A latent period of 0.37 *day* and a burst size of 20 were used as parameterized by the life history trait model (see Methods). The quadratic mortality terms are in $.(\mu molN.L^{-1})^{-1}.d^{-1}$.

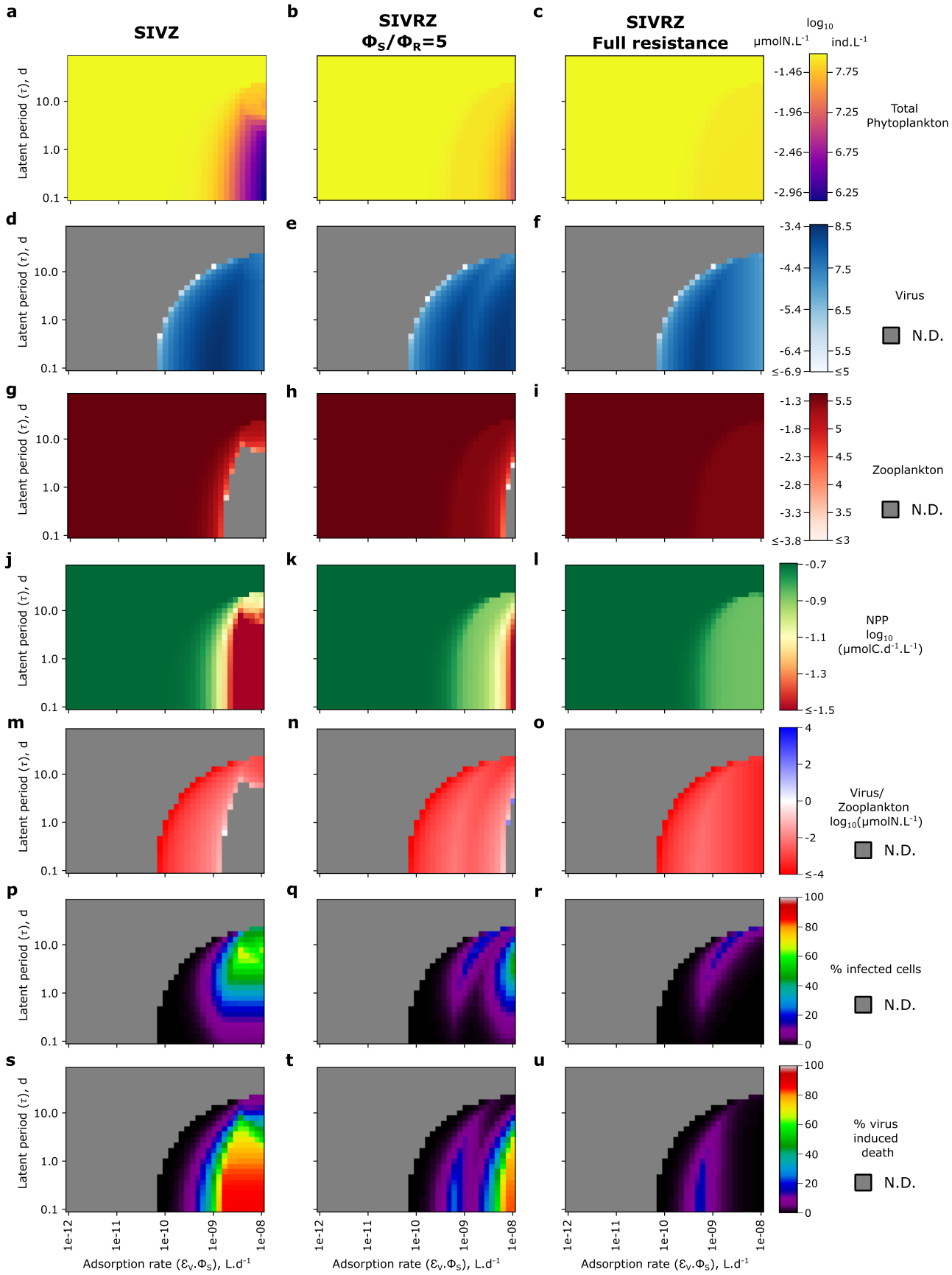

Figure 5 | Equilibrium concentration and ecological features of of the $SIVZ$ and the extracellular $SIVRZ$ models for *Prochlorococcus* across the adsorption rate and latent period parameter space. From left to right panels: $SIVZ$ model, $SIVRZ$ model with a partially resistant type: $\frac{\phi_S}{\phi_R} = 10$, and $SIVRZ$ model with a fully resistant type. (**a-c**) Total phytoplankton concentration. (**d-f**) Virus concentration. (**g-i**) Zooplankton concentration. (**j-l**) Ratio of virus to zooplankton concentrations. (**m-o**) Percentage of infected cells. (**p-r**) Percentage of virus induced death. In panels (**m**–**o**), the grey areas fall outside the coexistence domain, so these metrics are not defined. N.D.: Not Defined: the tracer is excluded or one of the necessary tracer to define the metric is excluded.

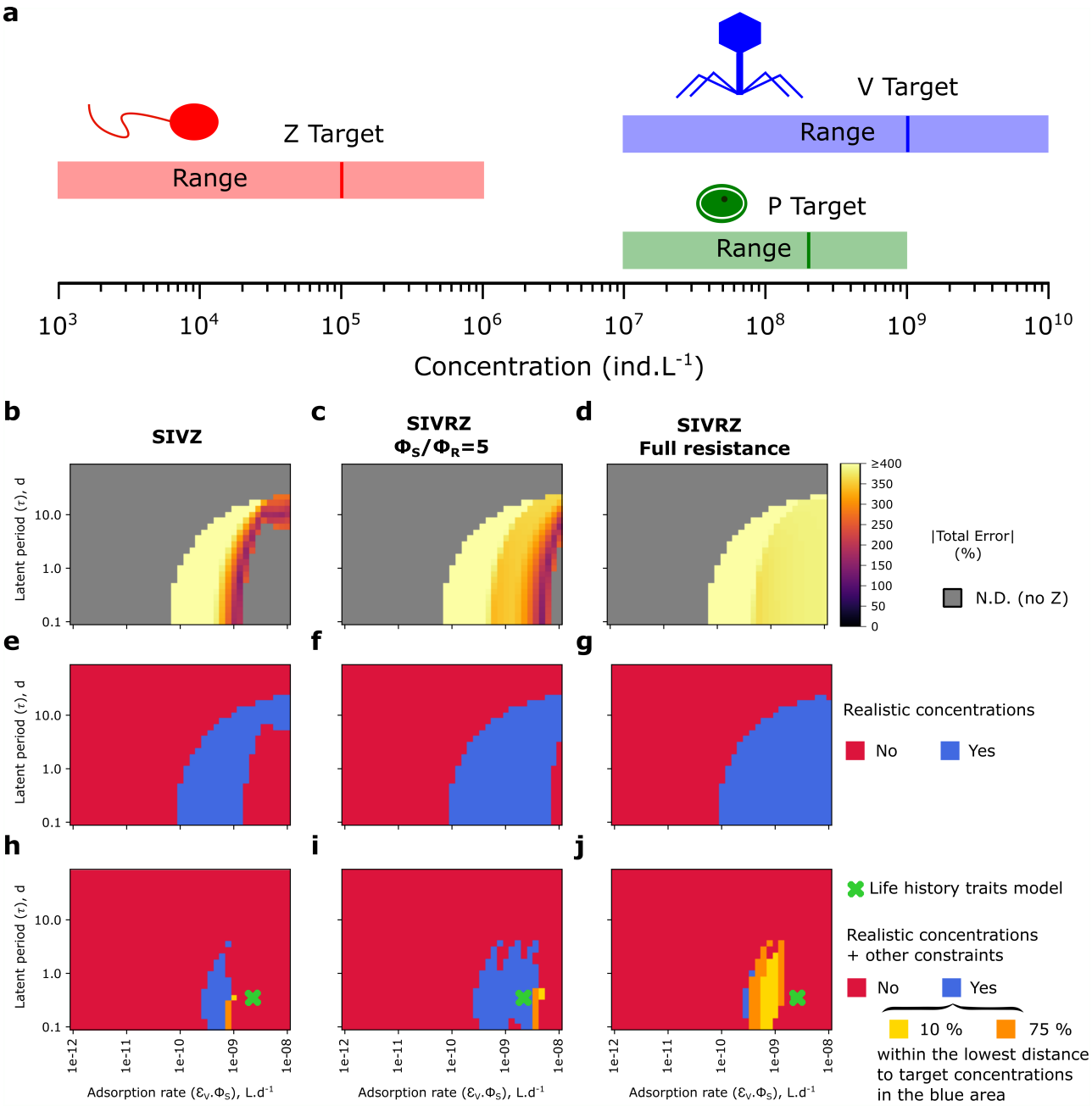

Figure 6 | Model output compared to expected concentration and ecological features measured in the field across the adsoprtion rate and latent period parameter space. (**a**) Target and concentration ranges in a mesotrophic environment for the zooplankton (red), *Prochlorococcus* (green) and the virus (blue). (**b-d**) From left to right panels: $SIVZ$ model, $SIVRZ$ model with a partially resistant type: $\frac{\phi_S}{\phi_R} = 10$, $SIVRZ$ model with a fully resistant type: (**b-d**) Distance to target concentrations defined in Table S4, (**e-g**) Realistic concentrations in the range defined in Table S4 and (**h-j**) Realistic concentrations and constraints on other expected ecological features (percentage of infected cells, percentage of virus-induce mortality and V/P ratio, see Table S4). The green cross represents the life history traits model. N.D.: Not Defined: at least one tracer is excluded.

Variable		*Prochlorococcus*	*Synechococcus*	Picoeukaryote	Diatom
Adsorption rate ϕ_R $10^{-12} - 10^{-8}$	Best	$2.8.10^{-10}$	$2.8.10^{-10}$	$1.7.10^{-9}$	$2.2.10^{-10}$
	Range	$1.7.10^{-10} - 1.3.10^{-9}$	$1.7.10^{-10} - 2.8.10^{-9}$	$10^{-9} - 1.7.10^{-9}$	$10^{-10} - 10^{-8}$
Extracellular resistance $\frac{\phi_{th}}{\phi_R}$	Best	7.7	17	3.3	175
	Range	$1.7 - 13$	$1.7 - 28$	$3.3 - 5.4$	$3.8 - 380$
Intracellular resistance $\frac{1}{\epsilon_{VR}}$ $1 - 10^4$	Best	1.3	3.6	1.7	2.8
	Range	$1 - 10$	$1 - 16$	$1 - 7.7$	$1 - 60$
Resistance cost $1 - \zeta$ $0 - 0.5$	Best	0.05	0	0	0.5
	Range	$0 - 0.2$	$0 - 0.1$	$0 - 0.05$	$0 - 0.5$
Linear V mortality d_V $0.01 - 1$	Best	0.2	0.01	0.4	0.01
	Range	$0.01 - 0.2$	$0.01 - 0.1$	$0.01 - 1$	$0.01 - 0.05$
Quadratic V mortality d_{V2} $0 - 2000$	Best	300	70	1100	200
	Range	$10 - 1400$	$20 - 400$	$200 - 2000$	$40 - 1000$
Quadratic Z mortality d_{Z2} $2 - 30$	Best	16	30	16	16
	Range	$8 - 30$	$10 - 30$	$10 - 18$	$1.6 - 30$

Table 1 | Parameter optimization to target concentrations for an oligotrophic and a mesotrophic simplified epipelagic environment using the approximate theoretical equilibria for the four phytoplankton types. The best parameter value is defined as the one minimizing the average absolute total error across the two environments for a given phytoplankton. The parameter range reflect the minimum and maximum value of a parameter within the first 200 best-fitting models. Parameter ranges tested are indicated below each parameter. Adsorption rate is in $L.d^{-1}$, extracellular, intracellular resistance and resistance cost are unitless, linear mortality is in d^{-1} and quadratic mortality terms are in $(\mu molN.L^{-1})^{-1}.d^{-1}$. Parameters that are kept fixed are described in Table S1-3.

Ocean		*Prochlorococcus*	*Synechococcus*	Picoeukaryote	Diatom
Oligotrophic	Minimum total error (%)	58	4	28	114
	Error Range (%)	35 – 100	8 – 87	25 – 109	24 – 130
	Tot P	$1.5.10^8$ (+53%)	3.10^7 (+50%)	$1.3.10^7$ (+27%)	$4.5.10^5$ (−11%)
	V	5.10^8 (+1.5%)	$4.7.10^8$ (−6.5%)	10^8 (−0.2%)	$1.8.10^8$ (−8%)
	Z	$10.3.10^3$ (+3%)	10^4 (+0.1%)	$4.9.10^3$ (−1%)	$9.7.10^3$ (+95%)
	% Inf	3.7	1.2	3.4	3
	% V kill	0.5	0.24	0.4	0.14
	V/P	3.3	16	7.7	400
Mesotrophic	Minimum total error (%)	22	57	46	53
	Error Range (%)	7 – 66	3 – 81	13 – 59	17 – 226
	Tot P	$1.9.10^8$ (−6.6%)	$5.1.10^7$ (+1.2%)	2.10^7 (−0.4%)	$1.4.10^6$ (−27%)
	V	$8.5.10^8$ (−15.3%)	10^9 (+1.9%)	2.10^8 (−0.2%)	$9.7.10^8$ (−3%)
	Z	10.10^4 (−0.3%)	10^5(+0.4%)	$2.7.10^4$(−45%)	$3.8.10^4$ (−23%)
	% Inf	5.6	2.5	6.3	13
	% V kill	0.4	0.27	0.4	0.27
	V/P	4.5	27	10	690
Weighted Average	Minimum error (%)	40	30	40	74
	Error Range (%)	40 – 56	30 – 48	40 – 48	74 – 94

Table 2 | Model performances compared to target concentrations for a simplified oligotrophic and mesotrophic epipelagic environment for the four types of phytoplankton. The absolute percentage error (rows Best and Range) represents the total error across target environments cumulating errors to the target concentrations of the phytoplankton, the zooplankton and the virus. For each environment, the "minimum error" corresponds to the error of best model for which the average absolute error across environments is minimized. The "Range" reflects the minimum and maximum values of the first 100 best models. For $TotP$, V, and Z, the equilibrium value is indicated in $ind.L^{-1}$ and the minimum percentage error to the target is in parenthesis. For % Inf, % V Kill and V/P the equilibrium value is shown.